Growth of metal and semiconductor nanostructures using localized photocatalysts

Grant No. DE-FG02-05ER15632

Sandia National Laboratories/NM

Principal Investigator: John A Shelnutt
Distinguished Member of the Technical Staff
Surface and Interface Sciences Dept. 01114
Advanced Materials Laboratory
Sandia National Laboratories
1001 University Blvd SE
Albuquerque, NM 87106
Phone (505) 272-7160
Fax (505) 272-7077
Email: jasheln@sandia.gov

Program Manager: Dr. Raul Miranda
Office of Basic Energy Sciences

Signing Official: Jerry A. Simmons
Manager, BES/DMS&E Program
Manager, Energy Sciences Dept. 01130
Phone (505) 844-8402
Fax (505) 844-4045
Email: jsimmon@sandia.gov

Use of human Subjects: No
Use of Vertebrate Animals: No

John A Shelnutt Date

Jerry A. Simmons, Signing Official Date

BASIC ENERGY SCIENCES

SANDIA NATIONAL LABORATORIES

2.0 Table of Contents

3.0 Abstract

Our overall goal is to understand and develop a light-driven approach to the controlled growth of novel metal and semiconductor nanostructures and nanomaterials. In this photochemical process, bio-inspired porphyrin-based photocatalysts reduce metal salts in aqueous solutions at ambient temperatures when exposed to visible light, providing metal nucleation and growth centers. The photocatalyst molecules are pre-positioned at the nanoscale to control the location of the deposition of metal and therefore the morphology of the nanostructures that are grown. Self-assembly, chemical confinement, and molecular templating are some of the methods we are using for nanoscale positioning of the photocatalyst molecules. When exposed to light, each photocatalyst molecule repeatedly reduces metal ions from solution, leading to deposition near the photocatalyst and ultimately the synthesis of new metallic nanostructures and nanostructured materials. Studies of the photocatalytic growth process and the resulting nanostructures address a number of fundamental biological, chemical, and environmental issues and draw on the combined nanoscience characterization and multi-scale simulation capabilities of the new DOE Center for Integrated Nanotechnologies at Sandia National Laboratories and the University of Georgia. Our main goals are to elucidate the processes involved in the photocatalytic growth of metal nanomaterials and provide the scientific basis for controlled nanosynthesis. The nanomaterials resulting from these studies have applications in nanoelectronics, photonics, sensors, catalysis, and micromechanical systems. Our specific goals for the past three years have been to understand the role of photocatalysis in the synthesis of dendritic metal (Pt, Pd, Au) nanostructures grown from aqueous surfactant solutions under ambient conditions and the synthesis of photocatalytic porphyrin nanostructures (*e.g.*, nanotubes) as templates for fabrication of photo-active metal-composite nanodevices. The proposed nanoscience concentrates on two thematic research areas: (1) the creation of metal and semiconductor nanostructures and nanomaterials for realizing novel catalytic phenomena and quantum control, (2) understanding photocatalytic metal deposition processes at the nanoscale especially on photocatalytic porphyrin nanostructures such as nanotubes, and (3) the development and use of multi-scale, multi-phenomena theory and simulation for ionic self-assembly and catalytic processes.

4.0 Narrative

4.1 Background and Significance

A. Previous results on photocatalytically nanostructured noble metals

Generally, metal nanostructures are of considerable commercial interest because of their importance in catalysis, photochemistry, sensors, tagging, and optical, electronic, and magnetic devices. Metal nanostructures have been synthesized in many forms, ranging from conventional metal colloids to modern near-monodispersed nanoclusters, shape-controlled nanocrystals, and other nanostructures such as wires and sheets. Nanostructured platinum is of particular interest for many applications, including catalysis, sensors, fuel cells, and other devices. While a few platinum nanostructures have been reported, including nanoparticles, nanowires, nanosheets, and others, the synthesis of additional types of nanostructures is highly desirable and potentially technologically important.

New methods for the synthesis of metal nanostructures are needed to provide the desired reproducibility and control over properties required for advanced technological applications. A recognized goal of these new synthetic approaches is control over the composition, size, surface species, solubility, stability, isolability, and other functional properties of the nanostructures. For example, shape-controlled platinum nanocrystals have been synthesized by El-Sayed and coworkers[1] using a capping polymer material, giving mixtures of tetrahedral, cubic, irregular-prismatic, icosahedral, and cubo-octahedral nanoparticles. The shapes produced are determined by interfacially directed control over the relative growth rates of different crystalline faces.

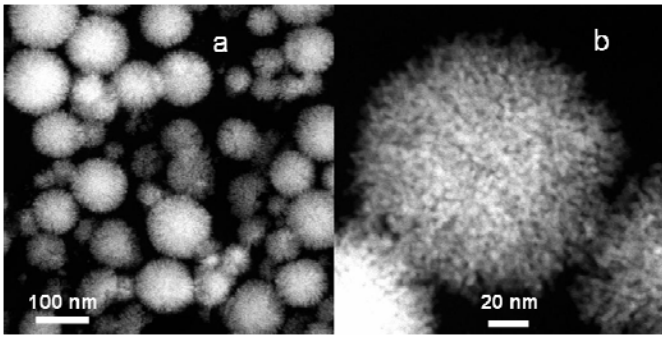

Figure 1. *HAADF scanning TEM image of the three-dimensional platinum dendrites grown in the presence of Brij-35 micelles and in the without photocatalyst.*

In the previous three years, we have demonstrated the viability of a new photocatalytic method for synthesizing metal and metal-composite nanostructures. The synthesis uses a porphyrin-based photocatalyst positioned inside surfactant assemblies for controlling the templated growth of novel platinum, palladium, and gold metal dendrites. These can be in the form of three-dimensional globular dendrites of controlled dimensions between 10-100 nm, which are produced in micellar solutions by altering the ratio of metal to photocatalyst and the amount of light exposure. (See Figs. 1 and 2) Alternatively, templating on liposomes containing the porphyrin photocatalyst molecules gives thin (~2-nm) flat circular metal dendritic sheets of 50-200-nm diameters (see below). When grown in aggregated liposomes, the nanosheets of platinum can produce foam-like metal materials, and the morphology of the metallic foams is easily controlled photocatalytically. The metallic dendrites were shown to be active catalysts for photocatalytic H_2 evolution from water and for the oxygen-reduction reaction in fuel cells.

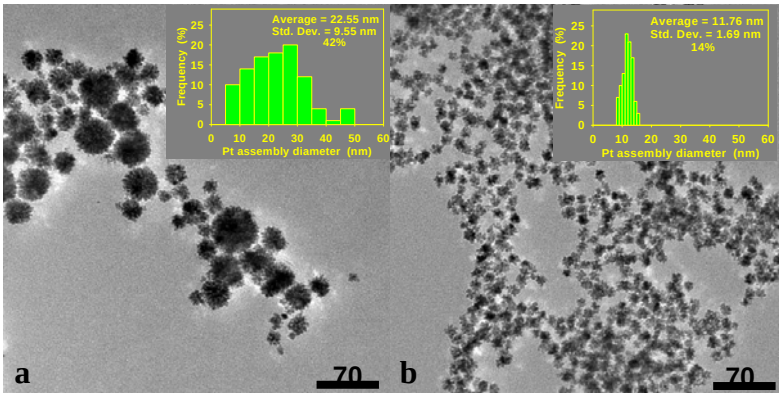

Figure 2. *TEM images of platinum nanostructures produced in the presence of SDS without (a) and with (b) photocatalyst and their respective size distributions (Insets). Average diameters were measured for 100 nanostructures and their frequencies are plotted in the inset graphs. The average size and the standard deviations are given in the plots, along with the percentage ratio of the standard deviation to average size.*

Our research is leading to new nanoengineered metals for catalysis including platinum, palladium, gold, and potentially other catalytically important metals. The metal nanostructures made by dendritic growth also have potential applications in nanoelectronic, nanophotonic, and nanomagnetic systems, and since they typically have attached photocatalytically active components they also may lead to new photoactive nanodevices. Our goal is to develop a fundamental understanding of the synthesis, uses, and limitations of these biomimetic photocatalysts and the

nanomaterials derived from them. The work has already led to relationships with industrial partners wishing to exploit these photocatalytic processes and the resulting nanomaterials. InfraSUR LLC is a small business that is licensing and further developing our photocatalytic metal reduction processes for environmental remediation. Praxair, BOC, and a startup company tentatively named NanoPhotoSynthetics are pursuing the development of solar hydrogen production methods based on nanodevices that may result from the photocatalytically derived nanostructures.

With the goal of synthetic control in mind, we have discovered and elucidated a method of synthesis that leads to novel types of fractal platinum nanostructures of controlled sizes. This synthetic method is based on a seeding and fast autocatalytic growth approach in which an aqueous solution of platinum salts is reduced by ascorbic acid in the presence of surfactant. Growth occurs by reduction of metal complex at the surface of the growing dendrite, not as is often the case by aggregation of metal nanoparticles. The seeding/autocatalytic growth approach employed by us produces nanodendrites like those shown in Fig. 1, which grow by interfacially directed autocatalytic reduction of platinum onto Pt nanoparticle seeds in an aqueous surfactant solution. Such metallic platinum nanodendrites had not been observed previously. We have developed a sufficient understanding of the chemical and photochemical processes involved in the formation of these platinum dendrites so that we can now control the nanostructure to a large extent. This understanding has been exploited to produce a wide variety of new metal nanostructures and nanomaterials, including Pt and Pd foam-like nanomaterials. In particular, we have clarified the use of the porphyrin photocatalysis to control the size and uniformity of these metal nanostructures.

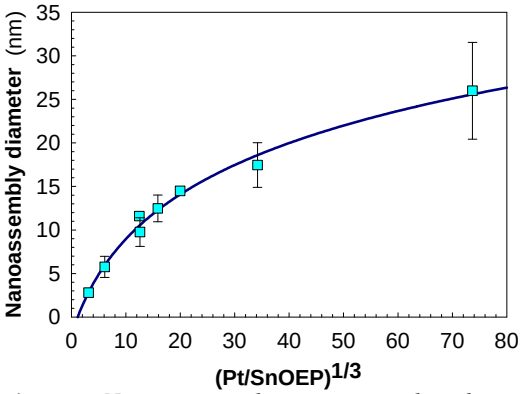

Figure 3. *Nanostructure diameter versus the cube root of the Pt-to-porphyrin molar ratio (a measure of the nanostructure volume per growth center).*

The photocatalytic reduction of platinum salts by the SnP, for example, is accomplished in the presence of visible light and ascorbic acid as an electron donor (ED). The SnP photoreaction is a reductive photocatalytic cycle, which has been used previously in the photoreduction of methylviologen and to evolve H_2 in the presence of colloidal Pt.[2, 3] In the present photoreaction, Pt^{2+} is reduced according to the following simplified equations:

$$SnP + h\nu \rightarrow SnP^*$$
$$SnP^* + ED \rightarrow SnP^{-\bullet} + ED_{ox}$$
$$2SnP^{-\bullet} + Pt^{2+} \rightarrow 2SnP + Pt^0.$$

Absorption of visible or UV light by the SnP yields the long-lived excited triplet π-π* state, SnP*, which is rapidly reduced (SnP*/SnP$^{-\bullet}$, +1.1 V) by an ED. The product is a long-lived (~10 seconds) radical anion, SnP$^{-\bullet}$, which is a strong reductant (SnP/SnP$^{-\bullet}$, -0.66 V) capable of efficiently reducing a variety of metal ions including Ag, Au, Hg, Pb, Cu, Pd, and Pt to the zero-valent metals. Reduction of the metal regenerates neutral SnP, which again becomes available to absorb light and initiate a successive photochemical cycle.

In the case of micellar surfactant solutions, slow reduction of Pt(II) by ascorbic acid yields seed nanoparticles that autocatalyze the metal reduction reaction by catalytic oxidation of ascorbic acid at the particle surface. The fast autocatalytic

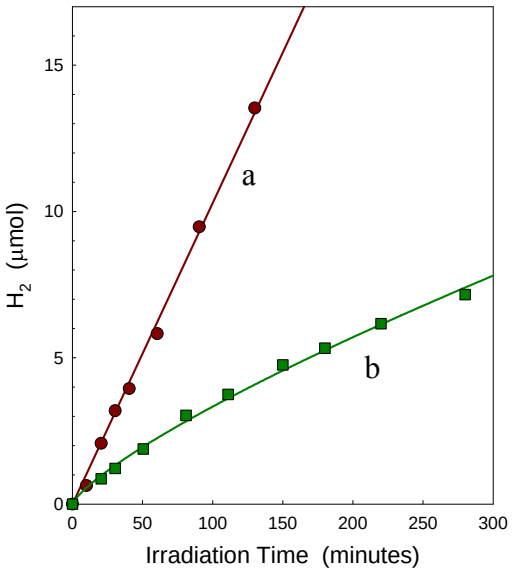

Figure 4. *Photocatalytic reduction of water to hydrogen by the platinum nanostructures, composed of the platinum nanodendrite, surfactant, and SnOEP, with added SnUroP (80 μM). The Pt nanostructures are diluted into an ascorbic acid (ED) solution containing the Sn uroporphyrin for the measurement. Water is reduced at rates as high as 6 μmol-hr^{-1} (H_2 turnover rate of 33 hr^{-1} in terms of SnUroP) by electrons from the Sn uroporphyrin anions supplied to the surface of the Pt catalyst. Incandescent white light intensity is 800 nmol-cm^{-2}-s^{-1}, but mostly light with wavelengths in the region of the Soret band of the porphyrin is absorbed. Reaction conditions are: (a) low Pt (6.5 μM) and high ascorbic acid concentration (200 mM) and (b) high Pt concentration (65 μM) with low ascorbic acid concentration (60 mM). H_2 turnover rates in terms of atomic Pt are (a) 390 hr^{-1} and (b) 14 hr^{-1}.*

growth from the seeds produces platinum dendrites with diameters ranging from 6 to 200 nm as shown in the scanning TEM image of Figs. 1 and 2a because slow reduction of Pt(II) by ascorbic acid produces small seed particles, which mature to a catalytic size at different times during the reaction. The surfactant micelles themselves can have negatively charged head groups (sodium dodecylsulfate, SDS) or polar headgroups (Brij-35), but surfactant is usually needed to obtain well formed spherical dendrites. These nanostructures were not initially recognized as dendrites, and their dendritic nature was only realized after similar dendritic sheets of platinum were discovered (see below).

When photocatalyst is present and the reaction mixture is exposed to light, the dendrite size is smaller and more uniform as shown in Fig. 2. Size control is conveniently realized by using a tin-porphyrin photocatalyst to rapidly generate a large initial population of growth centers, which thus have equal growth times before the Pt complex is exhausted. These seed particles grow by the rapid autocatalytic reduction of Pt(II), limited only by the amount of Pt(II) present in solution. The number of initial seed particle and thus the dendrite size can be controlled either by varying the concentration of the porphyrin photocatalyst under constant Pt(II) concentration and illumination conditions, by varying the light exposure at constant Pt(II) and porphyrin concentrations, or by varying the Pt(II) concentration at constant light and porphyrin concentration. For example, the effect of varying the photocatalyst concentration on the size of the dendrites is illustrated in Fig. 3. More porphyrin gives more seed particles and smaller average size of the dendrites. The size distribution is narrower because the photocatalytic seed generation effectively competes with seed generation by slow spontaneous reduction of Pt complex by ascorbic acid at the Pt surface.

This photocatalytic seeding approach can be used to produce dendrites with average sizes in the range of 10 to 50 nm with a narrow size distribution. At the highest photocatalyst concentrations, size can be reduced to the point where only 3-nm diameter Pt particles are formed. The effects of light exposure and porphyrin concentration on the size of the dendrites were fully evaluated in a full article in the *Journal of the American Chemical Society*.[4] Besides demonstrating the ability to control dendrite size, these studies fully support the proposed seeding/autocatalytic growth mechanism.

For the platinum nanodendrites in Fig. 2(b), we have demonstrated that they are functional catalytic/photocatalytic units capable of H_2 evolution from water (Fig. 4). The photocatalytically active porphyrin molecule likely remains associated with the nanostructure that it nucleated, and porphyrin can act reduce water to hydrogen in the presence of a sacrificial electron donor. Colloidal platinum is a well-known catalyst for H_2 evolution from water in artificial photosynthesis systems. The Pt nanostructure and the associated porphyrin photocatalyst is indeed able to generate H_2 in the presence of light and an electron donor in a manner analogous to the reaction mechanism described above for Pt(II) reduction, except that $SnP^{-\bullet}$ provides electrons to H^+ at the Pt metal surface to produce hydrogen,

$$2SnP^{-\bullet} + 2H^+ \xrightarrow{Pt} 2SnP + H_2 \cdot$$

The reaction mixture containing the (12-nm) platinum dendrites and associated porphyrin photocatalyst was irradiated with room light in the presence of ascorbic acid. After two months, the head-space of the sealed reaction vessel was analyzed by gas chromatography, and the presence of hydrogen was confirmed (~30% by volume). H_2 evolution is observed even in the presence of the surfactant coating on the nanodendrites. Also interesting is that the porphyrin delivers its reducing electrons directly to protons at the Pt surface without the aid of a relay molecule such as methylviologen that was sometimes used in

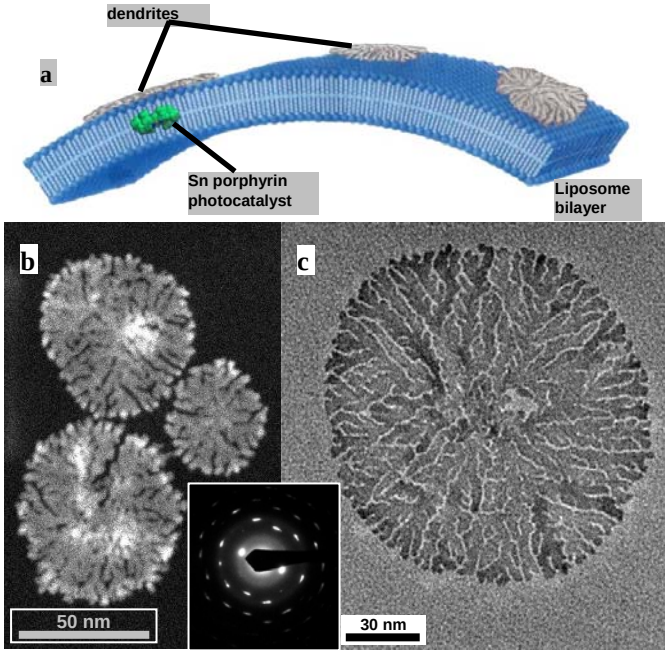

Figure 5. *Dendritic platinum sheets templated by liposomes. (a) Illustration of the growth of dendritic Pt nanosheets on the liposomal surface; the sheets may actually grow within the bilayer. (b) HAADF scanning TEM image of three platinum sheets grown on 160-nm DSPC liposomes. (c) TEM image of a dendritic Pt sheet on DSPC liposomes and (Inset) the electron diffraction pattern. The surfactant assemblies are not seen in the TEM images.*

previous studies.

The nanodendrite-porphyrin units suffer from poor light-harvesting capacity because of the low concentration of the light-absorbing porphyrin per dendrite and also the opacity of the colloidal suspension. To address these deficiencies, water-soluble Sn uroporphyrin was added to an ascorbic acid solution containing only a small amount of the dendrites. In this case, H_2 evolution is greatly accelerated, consistent with increased light flux and the additional light harvesting provided by the added tin porphyrins. As shown in Fig. 4, hydrogen evolution increases linearly for hours with turnover rates as high as 390 h^{-1} (mole H_2/mole atomic Pt). Given these findings, nanodendrites can be viewed as functional composite nanostructures consisting of the platinum dendrite, the adsorbed surfactant, and the associated active photocatalyst.

Other interesting Pt nanostructures can also be made using ascorbic acid reduction and photocatalytic seeding methods. For example, when large liposomes replace micelles as the template, dendritic disk-like sheets as shown in Fig. 5 or solid foam-like nanomaterials as shown in Fig. 6 are produced at the liposome surface. The Pt foams result from growth of the dendritic sheets or multiple aggregated liposomes. The particular nanostructure obtained depends on the solution conditions and size of the liposomes. The large cavities in the foams are determined by the liposome size.

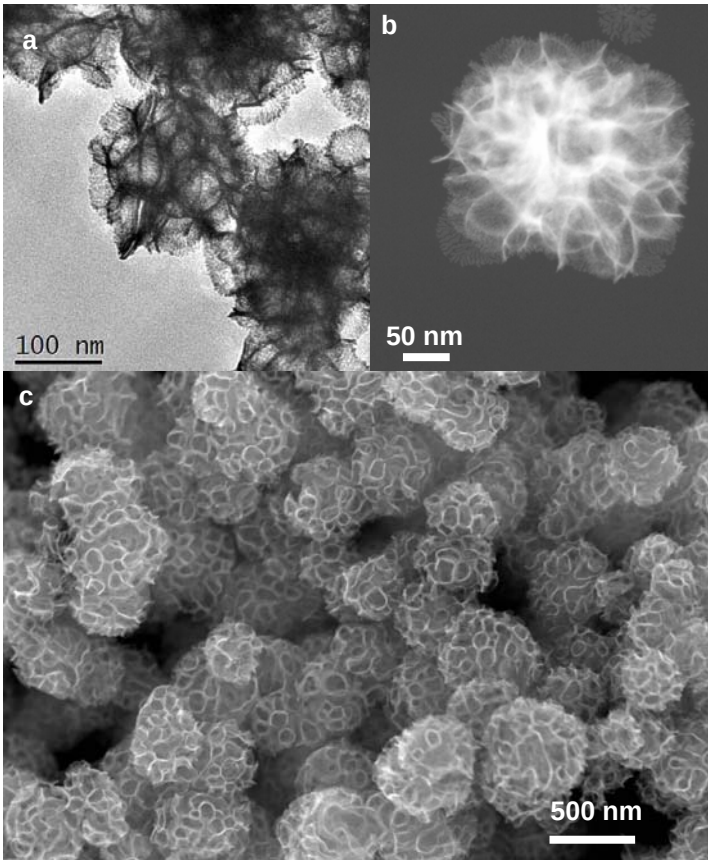

Figure 6. *Foam-like balls composed of platinum nanosheets grown over the bilayers of aggregated DSPC/cholesterol liposomes. The Pt foam balls can be grown with a uniform size using the porphyrin photocatalyst to initiate growth within the liposomal aggregates, and growth occurs on the liposomes in a spherically symmetric manner until the Pt(II) complex is exhausted. (a) TEM image, (b) HAADF scanning TEM image, and (c) SEM image of platinum nanofoams grown in the presence of 120-nm unilamellar liposomes. Reaction conditions: [Pt] = 10 mM; [AA] = 75 mM; [DSPC] = 0.25 mM; [cholesterol] = 0.25 mM.*

We have achieved additional control using a porphyrin photocatalyst as demonstrated previously for the globular dendrites. When the porphyrin photocatalyst is incorporated into the liposomes, exposure of the reaction solution to incandescent light produces small balls of the Pt foam (Fig. 6) and a more uniform ball size distribution. Varying the light exposure and porphyrin loading at constant platinum salt concentration determines the size of the foam balls and even gives continuous foam phases under certain conditions.

The platinum metal foams (Fig. 6) are also porous at a smaller scale than the diameter of the liposomes. The arms of the Pt dendrites (~2 nm thick; ~4 nm wide) on the liposomes are separated and have 1-2-nm spacings, providing small crevices through which small chemical species can pass. This porosity is most evident in the isolated circular sheets in Fig. 5b,c, which represent the corresponding 2-dimensional analogs.

The platinum metal foams have potential applications as catalysis because of their high surface area, our ability to control their porosity and conductivity on different length scales, and other possibilities for tailoring their structure. Fuel cells may be one commercial application in which the platinum nanofoams have advantages over existing systems. In this regard, the nanofoams shown in Fig. 6 are an uncommon example of a self-supported platinum nanostructure. The materials are highly porous and are expected to have good electrical connectivity because of the dendritic nature of the platinum. These features are highly desirable in applications such as fuel-cell electrocatalysts. An important property determining the potential of these materials as catalysts is the surface area, especially the electro-active surface area. Hence, we have determined the surface areas of the platinum nanofoams using nitrogen adsorption experiments and electrochemical CO stripping measurements.

The standard reaction using liposomes prepared in water was readily scaled by a factor of 100 compared to previous preparations to yield gram quantities of the Pt foam-like material, allowing us to determine the surface areas of the platinum nanofoams. The SEM images taken before and after washing and drying showed no evidence

of a significant structural change (data not shown). The washed nanofoam balls were subjected to DTA/TGA analysis to determine the purity of the material and to check for residual surfactant and water. The DTA/TGA diagram (not shown) quantifies the change in the weight of the sample and the temperature difference accompanying heat treatment in argon. Below 100 ºC, the weight change can be attributed to the release of adsorbed water molecules, whereas above 100 ºC the weight loss corresponds to the pyrolysis of organic molecules (presumably surfactants) still present in the platinum nanofoam. The sample, including adsorbed water and organics is > 97% platinum by weight.

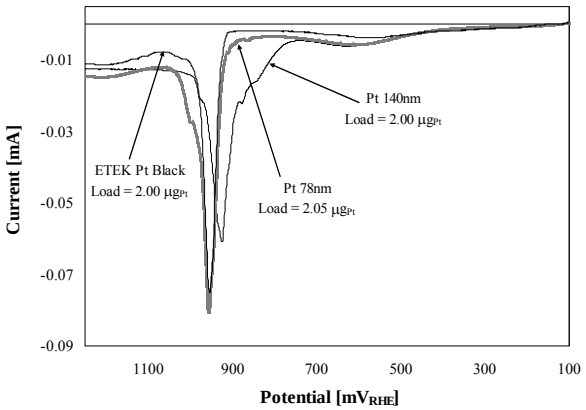

Figure 7. *Representative CO stripping voltammograms for Pt black, and the Pt foams formed with 140-nm and 78-nm liposomes. CO was adsorbed onto Pt at 100 mV_{RHE} in a CO saturated 0.5 M H_2SO_4 solution while rotating an RDE at 1000 rpm. The potential was then swept positive at 20mV/s to oxidize the adsorbed CO. The peak position and shape was found not to influence the calculation of the charge.*

The surface area of the platinum nanofoams is an important determinant of their catalytic activity and it has been measured using nitrogen adsorption experiments (data not shown). The platinum nanofoams made with 78-nm and 140-nm liposomes have similar surface areas of 26.9 ± 0. 5 m^2/g, based on repetitive N_2 adsorption experiments. This is comparable to the surface areas of the currently available commercial platinum black preparations for fuel cell applications, which are composed of particles with average diameters of 5-6 nm. Ozone plasma treatment for one hour, which should decompose any surfactant remaining on the surfaces of the platinum foam balls, gave identical BET surface areas.

For active surface area measurements, thin films of Pt nanofoams made with 140-nm and 78-nm liposomes in Nafion were prepared and initial cyclic voltammetry (CV) experiments were performed in N_2 sparged 0.5 M H_2SO_4. The CVs (not shown) exhibit features associated with hydrogen adsorption and desorption events at potentials *ca.* 100-200 mV_{RHE}; these features are characteristic of thin Pt films and polycrystalline Pt.[5]

Analysis of hydrogen adsorption/desorption events yield electroactive surface areas, as can the CO stripping experiments performed in this work. Representative CO stripping voltammograms for the three materials tested (140-nm and 78-nm Pt foams and ETEK Pt black) are shown in Fig. 7. The peaks at 900-1000mV_{RHE} are attributed to current being passed as CO that is adsorbed on the electroactive Pt surface (Pt-CO) is stripped away (oxidized) according to the following reaction:

$$Pt\text{-}CO + H_2O \rightarrow CO_2 + 2H^+ + 2e^-.$$

The exact shape and position of the peak changes without any observable trend and is not important in this study. The important parameter is the charge (Q) resulting from the CO oxidation event, which is calculated by integrating the background subtracted current as a function of time. Q is plotted *versus* Pt loading for ETEK Pt Black, 140-nm and 78-nm foams in Fig. 8. If the data is regressed with a zero intercept, the electroactive surface area ($SA_{e\text{-}active}$) can be calculated as follows:

$$SA_{e\text{-}active} = 1{,}000 * Slope * N_A/F * XSA_{Pt}/n,$$

where Slope [=] $mC/\mu g_{Pt}$, N_A = Avogadro's number (6.022×10^{23} atoms/mol), F = Faraday's constant (96,486 C/mol-e^-), XSA_{Pt} = atomic cross-sectional area of a Pt atom (8.00×10^{-20} m^2/atom), n = number of electrons in CO oxidation reaction ($2e^-$), and 1,000 is a metric conversion factor. The values for the $SA_{e\text{-}active}$ are reported in Fig. 8. The three samples have nominally

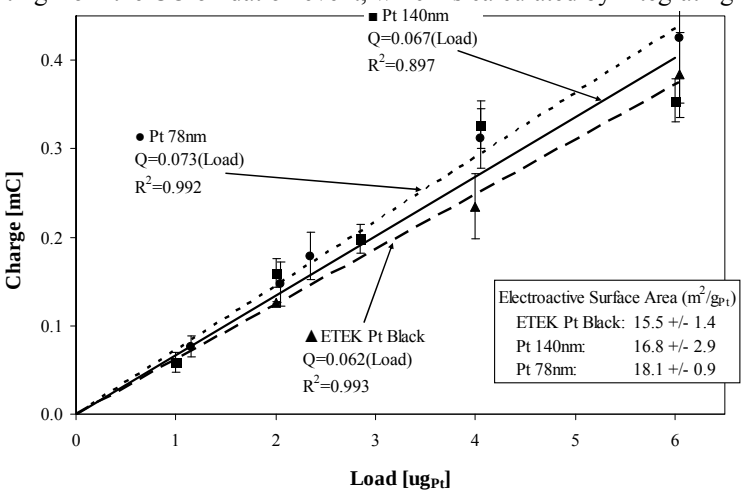

Figure 8. *Charge calculated from CO stripping (an example of which is shown in Figure 12) as a function of Pt loading onto a GCE (error bars represent one standard deviation). Electroactive surface area can be calculated from the slope of the line; those values are shown in the inset for Pt Black, Pt 140 nm and Pt 78 nm.*

the same $SA_{e\text{-}active}$, though Pt foam generated with the 78-nm liposomes does have a (statistically significant) greater $SA_{e\text{-}active}$ than the ETEK material. Achieving similar, if not slightly larger, electroactive surface areas in a structured Pt black material *versus* nanoclusters of unsupported Pt is, to the best if our knowledge, unprecedented in the literature.

The oxygen reduction reaction (ORR) was also probed via rotating disk electrode (RDE) experiments to see which of the following two reactions each Pt material catalyzes:

$$O_2 + 2H^+ + 2e^- \leftrightarrow H_2O_2$$
$$O_2 + 4H^+ + 4e^- \leftrightarrow 2H_2O.$$

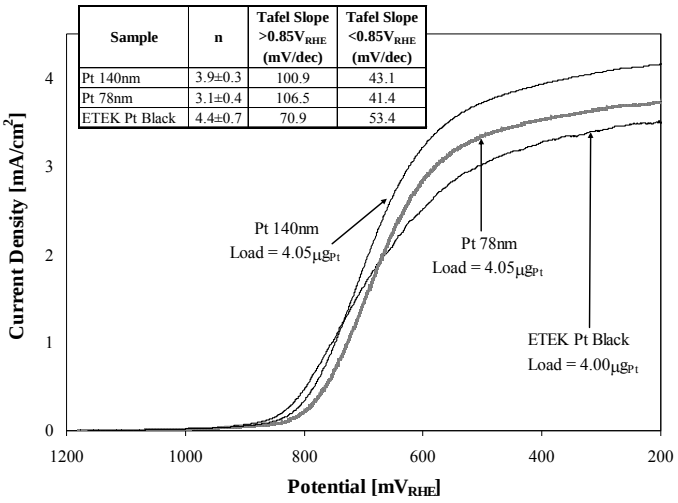

Figure 9. *Representative ORR curves for Pt Black, Pt 140 nm and Pt 78 nm. The potential was swept from 1265 to 165 mV_{RHE} at 5 mV/s in an O_2 saturated 0.5 M H_2SO_4 solution. The inset contains values for the number of electrons participating in the ORR and the mass transfer corrected Tafel slopes.*

The $4e^-$ reduction to H_2O is preferred over the reduction to H_2O_2, which lower the operating potential of the cell and degrades the stability of the materials. Fig. 9 shows ring-disk-electrode (RDE) polarization curves for ETEK Pt Black, 140-nm and 78-nm foam balls; the potential was swept at 5mV/s in an O_2 saturated 0.5 M H_2SO_4 solution. The lower the onset potential is at a given current density, the more facile the kinetics are for the ORR. Examination of Fig. 9 shows that the ETEK material performs better at high potentials (>700mV_{RHE}) while the 140-nm and 78-nm materials perform better at lower potentials (<700mV_{RHE}). Levich plots ($1/i_{lim}$ versus $\omega^{-1/2}$, where i_{lim} is the mass transfer limited current and ω is the rotation rate, not shown) were prepared from the ORR data to calculate n (the number of electrons in the ORR) from the Levich slope, which is determined from the following equation:

$$\text{Levich Slope} = [0.62nFACD^{2/3}\nu^{-1/6}]^{-1},$$

where Levich Slope [=] $mA^{-1}\ s^{-1/2}$, F is again Faraday's constant, A = geometric surface area (0.0707 cm^2), C = O_2 solubility in 0.5 M H_2SO_4 ($1.22x10^{-6}$ mol/cm^3),[6] D = diffusion coefficient ($1.04x10^{-5}$ cm^2/s),[6] and ν = kinematic viscosity ($9.87x10^{-3}$ cm^2/s).[7] Using these literature values and the Levich Slope, n was calculated and is reported along with the mass transfer corrected Tafel slopes in Fig. 9. The Tafel slope is found by plotting $Ln(i_k)$ versus potential where i_k is:

$$i_k = \text{kinetic current} = (i_{lim} \cdot i)/(i_{lim} - i),$$

and i is the measured current. Both ETEK Pt Black and the 140-nm foam follow the $4e^-$ reduction, as expected, while the higher surface area 78-nm foam has a value statistically less than 4. The Pt nanofoams, both 78 nm and 140 nm, have larger Tafel slopes above 850 mV_{RHE} and smaller Tafel slopes below 850 mV_{RHE} compared to the ETEK Pt Black. (*N.B.* The Tafel slopes reported in Fig. 9 are for the experiments shown in Fig. 9 only, but are representative of all experiments performed. Conversely, the reported values for n are for experiments performed on 4 different electrodes for each material tested, each at a different loading and probed at rotation speeds from 500-2500rpm). Typical Tafel slopes for Pt black materials are reported to be ~60mV/dec and ~120mV/dec;[5, 8] the difference between our values and those reported in the literature is likely due to different experimental conditions. In summary, the electrochemical experiments show that these nanostructured Pt foams catalyze the reduction of oxygen nominally as well as the Pt black nanoclusters of comparable surface areas.

We have made some progress on the use of photocatalytic metal reduction as a means for removing heavy metals from water. The work has focused on two areas—identifying an electron donor compatible with environmental uses and determining which metals may be removed and to what level. A small business (InfraSUR LLC) is developing this method of waste remediation under the name NanoMOR with the intention of commercializing a reactor based on the process. The efforts this year have focused on using benign electron donors like ethanol, which is already used for purification of municipal water supplies, and on removing Cr(VI), which is

removed by the process to undetectable levels. A provisional patent has been filed by the UNM, Sandia, and InfraSUR.

B. Metal Growth on Porphyrin Nanostructures and other Templates for Light Active Nanodevices

Porphyrins and other tetrapyrroles such as chlorophylls play important functional roles in biological nanostructures and proteins of photosynthetic systems. The porphyrins in biology are sometimes self-organized into nanoscale superstructures that perform essential light-harvesting and energy- and electron-transfer functions, and similar types of porphyrin structures might serve as a way of localizing porphyrin catalysts at the nanoscale onto which we might grow metals to produce nanoscale devices. A relevant example of the biological nanostructures formed by porphyrins is the light-harvesting bacteriochlorophyll rods of the photosynthetic pseudo-organelles of green-sulfur bacteria, called chlorosomes. The chlorosomal rods are composed entirely of aggregated bacteriochlorophyll molecules as illustrated in Fig. 10.[9-12] Because of their desirable functional properties, porphyrins (and other tetrapyrroles related to chlorophyll) are attractive building blocks for a wide variety of functional synthetic nanostructures.

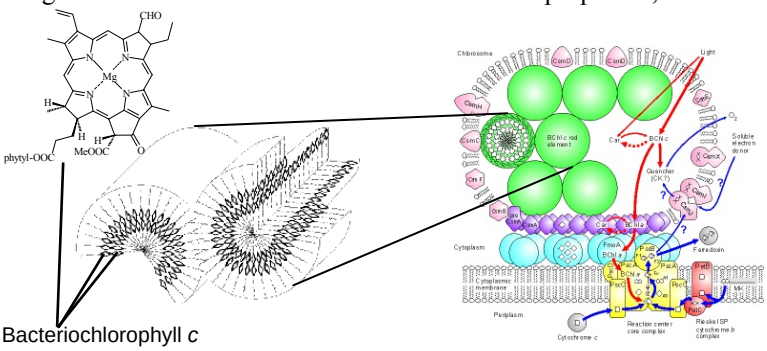

Figure 10. *Illustration of a chlorosome, which contains the chlorosomal rods that harvest light in green sulfur bacteria.*

The synthesis of new functional self-assembled nanostructures analogous to the chlorosomal rods, which have well-defined shapes and dimensions are of great current interest for applications in electronics, photonics, light-energy conversion, and catalysis, and they might also serve as additional templating nanomaterials for photocatalytic growth of metals and semiconductors to produce nanodevices. Porphyrins are attractive building blocks for these nanostructures because of their inherent electronic, optical, and catalytic properties.

Synthetic Porphyrin Nanostructures. During the first funding period for this contract, we discovered that photocatalytic porphyrin nanotubes can be prepared by ionic self-assembly of two oppositely charged porphyrins in an aqueous environment. These sturdy nanotubes represent a new class of porphyrin nanostructures, for which the molecular building blocks can be altered to control their structural properties. The nanotubes are photocatalytic, mechanically responsive and adaptive to light, and they exhibit other interesting electronic and optical properties. Most relevant for the continuing research for this contract, some of the porphyrin nanotubes photocatalytically reduce metal ions from aqueous solution and deposit the metal onto tube surfaces selectively, producing novel composite metal nanostructures that have potential applications as nanodevices. The nanotubes also serve as a platform for investigation of the metal reduction and deposition process at the nanoscale, especially the role played by the tube surfaces and adjacent solution interfacial layers.

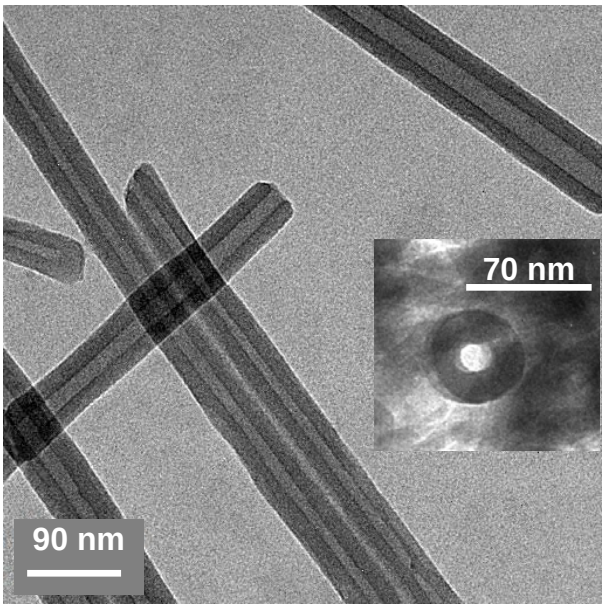

Figure 11. *TEM image of the porphyrin nanotubes using the porphyrins in Fig. 12. Inset: A tube trapped in a vertical orientation by a thick mat of tubes.*

The nanotubes shown in Fig. 11 represent the first porphyrin nanostructures that possess well-defined morphologies,[13, 14] and they may mimic the function of the chlorosomal rods. Their robustness makes them suitable for incorporation into nanodevices, such as for solar water splitting.[14] The nanotubes are biomimetic since the porphyrins are related to the chlorophyll molecules contained in systems found in nature that carry out light harvesting, charge separation and energy generation.[9-12] In fact, the porphyrin nanotubes in Fig. 11 appear to mimic both the light-harvesting and reaction-center functions of chlorosomes (Fig. 10).

Our robust porphyrin nanotubes are prepared by

ionic self-assembly[15] of two oppositely charged porphyrins in aqueous solution and are composed entirely of porphyrins such as those shown in Fig. 12. The nanotubes are one member of a new class of porphyrin-based nanostructures (see below) that we are developing, for which the molecular building blocks (tectons) can be altered to control their structural and functional properties. The porphyrin nanotubes obtained are hollow structures with uniform diameter and shape of nanoscale dimensions. The strong electrostatic forces between these porphyrin tectons add to the van der Waals, hydrogen-bonding, axial coordination, and other weak intermolecular interactions that typically contribute to the formation of porphyrin aggregates, enhancing the structural stability of these nanostructures.[16, 17]

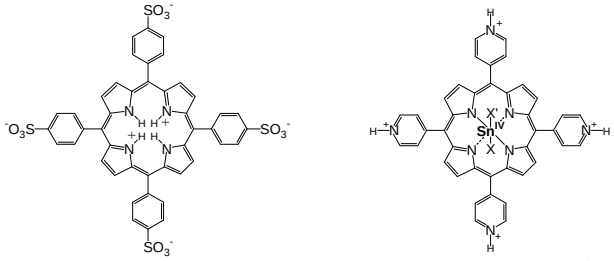

Figure 12. *Porphyrins used in making the porphyrin nanotubes shown in Fig. 3. The Sn(IV) center will have ligands (X, X′ = Cl, OH, H_2O) bound above and below the porphyrin plane. At pH 2 where the tubes are assembled, X = OH and X′ = H_2O (net charge +5) or X = X′ = OH (net charge +4).*

Specifically, the porphyrin nanotubes in Fig. 11 are formed by mixing aqueous solutions of two porphyrins (Fig. 12) such as the dication of *meso*-tetrakis(4-sulphonato-phenyl)porphyrin ($H_4TPPS_4^{2-}$) and Sn(IV) tetrakis(4-pyridyl)porphyrin ($SnTPyP^{2+}$) dichloride. Typically, 9 mL of freshly acidified $H_4TPPS_4^{2-}$ solution (10.5 μM $H_4TPPS_4^{2-}$, 0.02 M HCl) was mixed with 9 mL of $SnTPyP^{2+}$ in water (3.5 μM $SnTPyP^{2+}$) and the mixture was left in the dark at room temperature for 72 hours, giving a 90% yield of nanotubes. When the Sn(IV) complex is replaced with other six-coordinate metal ions (*e.g.*, Fe(III), Co(III)) tubes are also obtained, thus the metal complexes can be varied to alter functional properties of the tubes.

The tubes can be micrometers in length and have diameters in the range of 50-70 nm, with approximately 20-nm thick walls for the tubes formed using the 4-pyridyl Sn porphyrin. The tubes have a smaller average diameter of 35 nm when the 3-pyridyl Sn porphyrin is used instead. Images of the nanotubes caught in vertical orientations (Fig. 11, Inset) confirm a hollow tubular structure with open ends rather than a solid cylindrical structure.

Porphyrin-Nanotube Metal-Composite Nanostructures. Besides potentially possessing some of the useful activities of their biological counterparts, we have also found that the porphyrin nanotubes possess other remarkable features, including the ability to self-metallize and form nanotube-metal composites.[13] These new composite nanostructures offer the exciting possibility of making nanoscale devices that employ the photocatalytic and photonic properties of the nanotubes. Such nanodevices encompass many of the desired features of next generation devices for solar hydrogen production, such as nanoscale feature sizes, novel light-harvesting and photoconversion components, and the use of tunable organic semiconductors. Our development of porphyrin nanostructure-metal composites represents a technological breakthrough that may lead to a variety on new photonic and photocatalytic nanodevices. The nanotubes shown in Fig. 11 are made with a tecton (*i.e..,* the tin porphyrin shown in Fig. 12) that confers photocatalytic activity, as well as mechanical responsiveness to light. These porphyrin nanotubes also have other interesting electronic and optical properties such as intense resonance light scattering arising from the *J*-aggregate structures forming the tube walls.

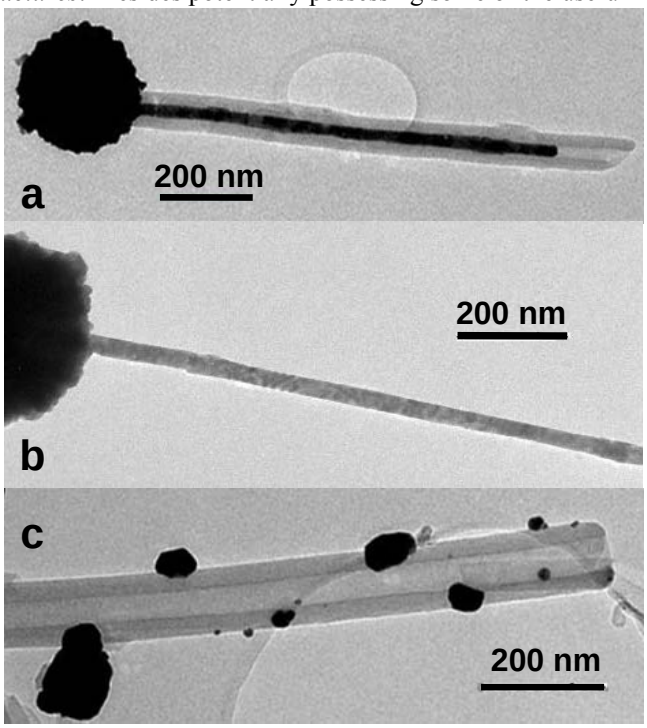

Figure 13. *Transmission electron microscopy images of (a) a gilded nanotube obtained using the Au(I) thiourea complex, (b) a gold wire obtained after the porphyrin tube has been dissolved away at pH 10 by adding 0.05 M NaOH, demonstrating the structural integrity of the free standing nanowires, and (c) a tube decorated by gold nanoparticles obtained using Au(I) thiosulfate.*

An important feature of the tubes is that their photocatalytic activity can be used to construct nanoscale metal components that can serve various functions (catalysis, conductors) in light-active nanodevices. Specifically, the unique photocatalytic

properties of the porphyrin nanotubes have been used to grow composite metal nanostructures like those shown in Figs. 13 and 14. The photocatalytic reduction reaction mediated by Sn(IV) porphyrins has been investigated previously by us[3, 18, 19] and is described by the following simplified cyclic reactions for a Au(I) complex:

$$SnP + \hbar\nu \rightarrow SnP^*$$
$$SnP^* + ED \rightarrow SnP^{-\bullet} + ED_{ox}$$
$$SnP^{-\bullet} + Au^+ \rightarrow SnP + Au^0$$

In the cases of Au(I) thiourea or thiosulfate complexes that are transparent to visible light, metal reduction is predominately photocatalytic and is dominated by the strongly light-absorbing Sn-porphyrin-containing nanotubes using ascorbic acid as the electron donor (ED) in the above reaction. Although an insignificant amount of autocatalytic reduction of gold complex by ascorbic acid at the metal surface has not been excluded, no reduction of gold complex occurs without initiation by visible light irradiation in the presence of the Sn porphyrin containing nanotubes, and autocatalytic reduction is negligible on the 30-minute maximum time scale of the photocatalytic reaction that we employ.

The reduction of gold(I) ions by the porphyrin nanotubes illustrates both their unique photocatalytic properties and an unusual surface-selectivity in the gold deposition. The latter is beneficial in the use of the tubes in the construction of functional metal composite nanodevices. When the nanotubes photoreduce the Au(I)-thiourea complex, the metal is deposited exclusively within the hollow interior of the nanotubes, forming a continuous gold nanowire that is of the same diameter as the tube core (Fig. 13a). Only continuous gold wires are found, *i.e.*, multiple short segments of wire or particles are typically not observed in a single nanotube. In addition, the nanowire is typically terminated at one end of the nanotube with a gold ball (nanoparticle) of larger diameter than the tube. When the porphyrin nanotubes are dissolved by raising the pH, the free-standing gold wire and ball remain intact as shown in the Fig. 13b. In contrast the negatively charged Au(I) thiosulfate complex results in the formation of gold nanoparticles mostly on the outer surfaces of the tubes. Together, these results suggest remarkable inner-outer surface selectivity, possibly due to special electron-transport processes and energy-transport processes that are at play within the porphyrin *J*-aggregates making up the tube walls. Electron-transfer processes may also explain the remarkable mechanical response of the bare nanotubes to illumination with intense visible light, evidenced by their switching from tubular to flattened rod-like structures in the TEM images. This mechanical response is perhaps a result of photo-initiated intermolecular electron transfer, which would disrupt the charge balance and hence the structure of the porphyrin ionic solid. This partially reversible response to light illumination seems to be ameliorated to some degree when ascorbic acid is present, perhaps by allowing radical anions to form instead of charge transfer species.

The gold wire and the ball at the end of the tube might be used as an electrical connector between components of a nanoscale photoelectrochemical device. For example, the gold ball attached to an electrode might serve to conduct electrons to the porphyrin nanotube at a redox potential capable of reducing the Sn porphyrins in their excited state, thus replacing the electron donor in the above equation. The porphyrin anions generated in the tube might then be used to carry out photoreactions other than metal reduction.

Such composite nanostructures can also be made using other metals such as platinum and palladium. We described above how Sn porphyrins can be used as photocatalysts to control the growth of dendritic metals using ascorbic acid as ED. In the case of platinum, the metal grows as dendritic 2-nm thick sheets or as spherical dendrites depending on nature of the surfactant assembly (liposomes or micelles) upon which the growth is templated. The

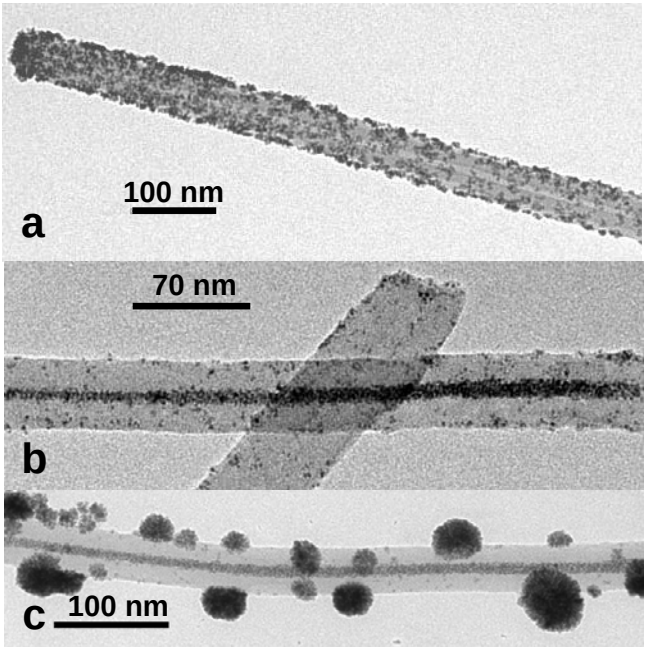

Figure 14. *Transmission electron microscopy images of (a) a platinized porphyrin nanotube with Pt nanoparticles distributed mainly on the outside surface, (b) a long Pt dendrite in the core of the tube obtained at a higher concentration of Pt complex, and (c), at a later stage in the development of (b) a long dendrite in the core and globular Pt dendrites on the outer surface of the nanotube.*

growth can also be controlled somewhat by photocatalytically producing seed particles. Similarly, platinum metal can be grown and deposited onto the nanotube surfaces (see Fig. 14) as photocatalytic initiation of growth by photoreduction of platinum complex gives small Pt seed nanoparticles on the tubes. These seed particles can decorate mainly the outer surfaces of the porphyrin nanotubes (Fig. 14a). Normally, fast autocatalytic reduction of Pt occurs after the seed particle reaches a certain size, producing Pt dendrites, and some small Pt dendrites are visible in this TEM image. Under different solution and irradiation conditions, we have also successfully grown long dendritic platinum wires within the cores of the nanotubes (Fig. 14b,c) and both Pt dendrites in the core and globular Pt dendrites on the outer surface (Fig. 14c).

Photosynthesis of Hydrogen in the Presence of an Electron Donor. The platinum nanoparticles on the porphyrin nanotubes act as a catalyst for photocatalytic water reduction, so that, in the presence of visible light and an electron donor such as ascorbic acid, the platinized nanotubes evolve hydrogen by the reaction:

$$2SnP^{-}\bullet + 2H^{+} \xrightarrow{Pt} 2SnP + H_2 .$$

H_2 production increases with increasing exposure to light (data not shown). Hydrogen production was measured by gas chromatography using a TCD detector. The platinum coverage and concentration of the nanotubes has not been optimized, and TEM images showed that few of the tube possessed platinum particles in this initial study. In addition, the colloidal nature of the platinized nanotube suspension and the intense resonance light scattering of the porphyrin nanotubes make accurately measuring the quantum yield for the formation of hydrogen difficult. Nevertheless, we can expect quantum yields for H_2 to approach 0.5 based on the photocatalytic reaction of Sn porphyrins in homogeneous solutions measured earlier.[3, 18]

C. BES long-term measures

This proposal directly addresses two of the four long-term BES performance measures. Specifically, the proposed work will demonstrate progress in the areas of (1) designing, modeling, fabricating, characterizing, analyzing, assembling, and using a variety of new materials and structures, including metals, alloys, and biomaterials at the nanoscale for energy-related applications and (2) understanding, modeling, and controlling chemical reactivity and energy-transfer processes in solutions, at interfaces, and on surfaces for energy-related applications by employing lessons from inorganic, organic, self-assembling, and biological systems.

4.2 Preliminary Studies

A. Metallic nanomaterials from porphyrin photocatalysts in surfactant assemblies and other templates

Our efforts toward gaining additional control of platinum, palladium, and gold nanostructures, which are produced on surfactant assemblies, are continuing to yield novel catalytic materials. For the platinum foam balls of the type shown in Fig. 6, we have measured the surface areas by N_2 adsorption and electrochemical CO stripping measurements. We are also currently testing the foam-like balls as electrocatalysts in PEM fuel cells. We plan to continue to characterize the catalytic properties of these and similar materials that we intend to make in the next funding period. We will mainly focus on determining the surface area, mass transport, and electrocatalytic activity of metal alloys made into dendritic sheets of various morphologies as was done for the pure Pt foam balls (Figs. 7-9). These new nanostructured materials might provide a cost-effective replacement for platinum as electrocatalysts in PEM fuel cells.

We have preliminary data on a new type of liposome-templated metal structure. Fig. 15 shows the result of precise control of the porphyrin and Pt complex concentrations and the light exposure to produce many small dendritic sheets in the liposomal bilayer, which are just the right size so that they grow together at the edges to produce a network of platinum 'daisies' that preserves the shape of the templating liposome. This new type of liposome-templated structure is expected to have high surface area, good mass-transport properties, and electrical conductivity and connectivity. It is one of the new nanomaterials that, like the Pt foam balls, is of interest for high current density fuel cell applications.

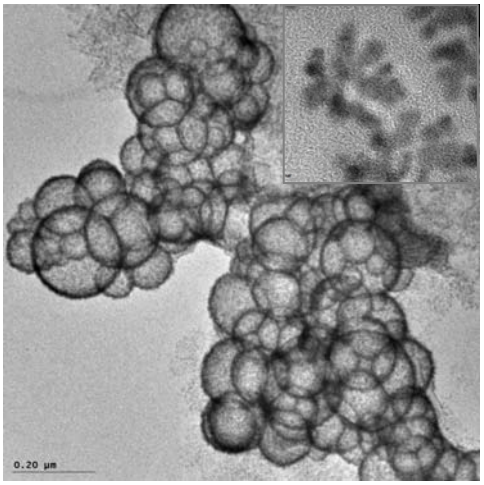

Figure 15. *Platinum dendritic 'daisies' (Inset) grown on liposomes to the point where they just touch and join adjacent daisies, thereby preserving the structure of the liposomes.*

We will also continue to investigate new templates for photocatalytic growth of metals. For example, we have found that microemulsions of organic solvents such as benzene in water can

provide a simple convenient template for metal growth. Fig. 16a shows platinum dendritic 'fur' grown on the surface of benzene droplets in water, where the benzene droplets have their surfaces coated with the photocatalytic lipoporphyrin shown in Fig. 16. The amount of platinum complex available and the light exposure can be adjusted so that the Pt fur can be made thin enough to give a platinum shell coating the benzene droplet (Fig. 16b). No attempt was made to control the size of the droplets, but as we can see from the smallest Pt-coated droplets in Fig. 16, we could easily make nanoscale metal spheres in this way.

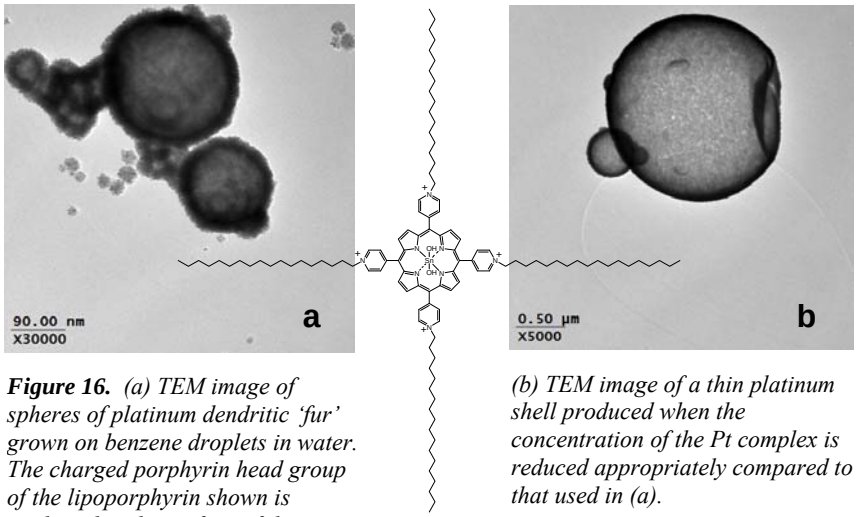

Figure 16. *(a) TEM image of spheres of platinum dendritic 'fur' grown on benzene droplets in water. The charged porphyrin head group of the lipoporphyrin shown is anchored at the surface of the droplets by the alkane tails, which freely dissolve in benzene. (b) TEM image of a thin platinum shell produced when the concentration of the Pt complex is reduced appropriately compared to that used in (a).*

B. Properties and characterization of the porphyrin nanotubes and their metal composites

For the porphyrin nanotubes, we intend to continue to investigate their optical and catalytic properties. We are also continuing efforts to gain additional control over their synthesis, in particular, control over size, morphology, and uniformity. For the metal composite nanostructures obtained from the porphyrin nanotubes, additional control over the deposition of metals, including precise deposition of different metals on the tubes, is desired for the fabrication of various nanodevices for catalysis, photosynthesis, and electronics and photonics applications. An attempt at the latter is shown in Fig. 17; the TEM image is of a nanotube containing a gold nanowire in the core and platinum nanoparticles on the outer surface. Our goals in this case are to obtain a high yield of gold wires exclusively in the tubes and a selectable uniform degree of coverage of individual Pt particles on the outer surface. Several synthetic methods of adsorption or growth of particles and wires are being examined. To realize the desired control over the exact structure of these composite nanostructures, we need to better understand the structures and properties of the nanotubes in greater detail.

Electron Microscopy. Transmission electron microscope (TEM) images of the porphyrin nanotubes (Fig. 11) reveal that they are micrometers in length and have diameters in the range of 50-70 nm with approximately 20-nm thick walls. Images of the nanotubes caught in vertical orientations (see Inset of Fig. 11) confirm a hollow tubular structure with open ends. Beyond these gross features, little is known about the packing of porphyrins within the ionic solid forming the tubes. However, we are beginning to obtain additional information, which may lead to the discovery of the detailed molecular structure of the tubes. For example, fringes with 1.7-1.8-nm spacings are seen both in end-on views and at the edges of the nanotubes in TEM images (data not shown). These fringes probably originate from the heavy tin and sulfur atoms in the porphyrin stacks. The fringes seen in the TEM images, combined with the optical spectral results discussed below, are consistent with a structure composed of stacks of offset *J*-aggregated porphyrins (the individual porphyrins are approximately 2 x 2 x 0.5 nm) possibly in the form of cylindrical lamellar sheets. The lamellar structure could be similar to an architecture proposed for the stacking of bacteriochlorophyll molecules in the chlorosomal rods.[10] X-ray diffraction studies (not shown) exhibit peaks in the low- and high-angle regions with line widths suggesting moderate crystallinity.

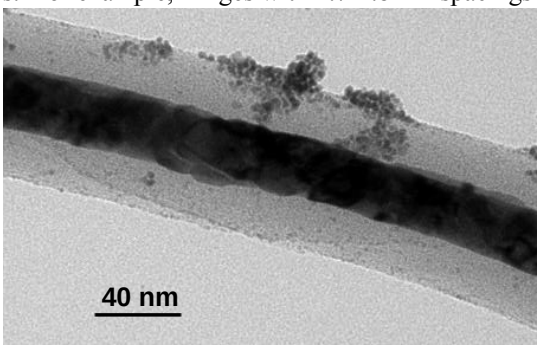

Figure 17. *Our initial fabrication goal is to prepare a gilded porphyrin nanotube with an optimum coverage of Pt particles. This high-magnification TEM image shows a porphyrin nanotube containing a gold wire in the core and some Pt nanoparticles on the outer surface, demonstrating that this is feasible.*

Atomic Force Microscopy. Additional imaging, spectroscopic techniques, and other property measurements are being brought to bear to gain further understanding of the structures and properties of the porphyrin nanotubes. For example, representative AFM images of the nanotubes are

shown in Fig. 18. These images were obtained in collaboration with Kevin Zavadil at Sandia National Laboratories. They are generated in intermittent contact ("tapping") mode in air using a Si cantilever with a tip curvature radius of less than 10 nm and a full tip cone angle of 30°. The nanotubes tend to agglomerate into mat-like domains when deposited from an aqueous solution onto a mica or Au-coated mica substrates. Despite agglomeration, individual tubes are imaged under these deposition conditions as shown by the 1 micron long, 23 nm diameter tube (probably collapsed) rotated by 30° counterclockwise in the upper portion of Fig. 18. This diameter measurement for tubes is in good agreement with the diameter for the individual tubes obtained from TEM images. We have also obtained preliminary STM images of the tube (not shown) in collaboration with Prof Ursula Mazur at Washington State University.

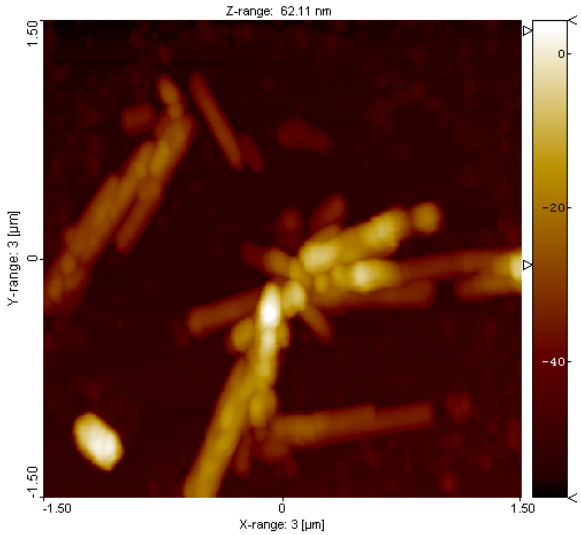

Figure 18. *Topography AFM image of porphyrin nanotubes obtained using the tapping mode of operation.*

Composition of the Nanotubes. The composition of the nanotubes has been determined by UV-visible absorption spectroscopy and energy dispersive X-ray (EDX) spectroscopy. The filtered nanotubes were dissolved at pH 12 and the ratio of the porphyrins was determined by spectral simulation using extinction coefficients for $H_2TPPS_4^{4-}$ (ε_{552} = 5500 $mol^{-1}dm^3cm^{-1}$) and $Sn(OH)_2TPyP$ (ε_{552} = 20200 $mol^{-1}dm^3cm^{-1}$), giving an approximate molar ratio of 2.4 $H_2TPPS_4^{4-}$ per $Sn(OH)_2TPyP$. EDX measurements of the S:Sn atomic ratio of the porphyrin tubes on the TEM grids also indicate a molar ratio of between 2.0 and 2.5. The observed ratio of the two porphyrins in the tubes (2.0-2.5) can be related to the charges of the porphyrin species present at pH 2 (see Fig. 12). As shown by acid-base titrations monitored by UV-visible spectroscopy (not shown), the porphyrin species present at pH 2 are $H_4TPPS_4^{2-}$ and a mixture of $Sn(OH)_2TPyP^{4+}$ and $Sn(OH)(H_2O)TPyP^{5+}$ (formed by protonation of the pyridine substituents of $Sn(OH)_2TPyP$ and, in the latter species, by the additional replacement of one OH^- axial ligand with H_2O at low pH). The formation of the nanotubes critically depends on the pH (*e.g.*, they are not formed at pH 1 or 3), as expected because the charge balance of the ionic tectons depends on their protonation state. EDX spectra of the nanotubes also showed no evidence of significant amounts of Cl (or I when HI was used in place of HCl), precluding the presence of chloride as counter ions, axial ligands, or salt bridges. So far, we cannot rule out the presence of water molecules (in addition to those present as axial ligands) that might play a structural role in the nanotubes. As expected for a nanostructure formed by ionic self-assembly, the same ratio of porphyrins (2.0-2.5) is observed in the nanotubes regardless of the initial ratio of the two porphyrins in solution.[14] Additional studies are needed to determine the role for various intermolecular interactions (electrostatic, H-bonding, van der Waals, etc.) in the formation of these nanotubes and other porphyrin nanostructures (see below).

Optical Properties. Besides their use as photocatalysts, the porphyrin nanotubes exhibit some other interesting and potentially useful optical properties. For example, the porphyrins in the nanotubes are stacked in a manner that produces UV-visible absorption bands at 496 and 714 nm; these are strongly red-shifted from the corresponding bands of the monomeric porphyrins (Fig. 19). These bands indicate the formation of *J*-aggregates similar to those of $H_4TPPS_4^{2-}$ and other porphyrins,[16, 17, 20] but the bands of the nanotubes are broader than those of the self-aggregates of $H_4TPPS_4^{2-}$, suggesting that the coherent coupling of the transition dipoles spans fewer molecules than the 10-20 molecules estimated for $H_4TPPS_4^{2-}$ self-aggregates.[20] The *J*-aggregate bands of the nanotubes result in intense resonant light scattering at these wavelengths, making the nanotube suspension appear bright green due to the resonance scattering under intense white light illumination, but light greenish yellow in weak transmitted light. In addition, the strong fluorescence of the porphyrin monomers is strongly quenched in the nanotubes.

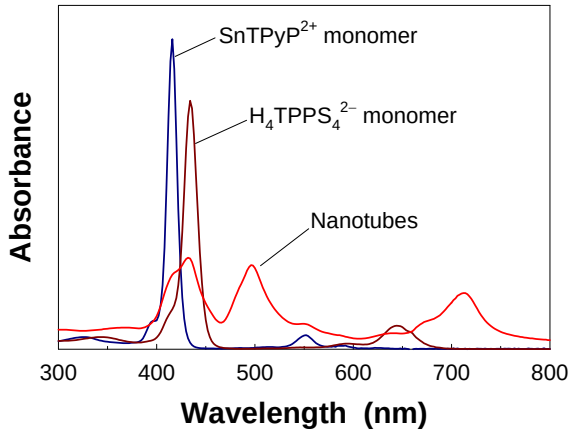

Figure 19. *UV-visible absorption spectra of a colloidal suspension of the porphyrin nanotubes and the constituent porphyrin monomers.*

Photosynthesis of hydrogen by platinized

porphyrin nanotubes. We have found that platinum nanoparticles on the porphyrin nanotubes, as shown in Fig. 14a, add the catalytic activity required for water reduction to hydrogen, and thus a platinized tube constitutes a viable component of a nanodevice for photocatalytic water reduction. In the presence of visible light and a sacrificial electron donor such as ascorbic acid the platinized nanotubes evolve hydrogen. This presumably occurs because of the ascorbic acid reduction of the excited tin porphyrins in the nanotubes in the presence of light, ultimately producing porphyrin radical anions that reduce protons at the Pt-nanoparticle surface to produce hydrogen.

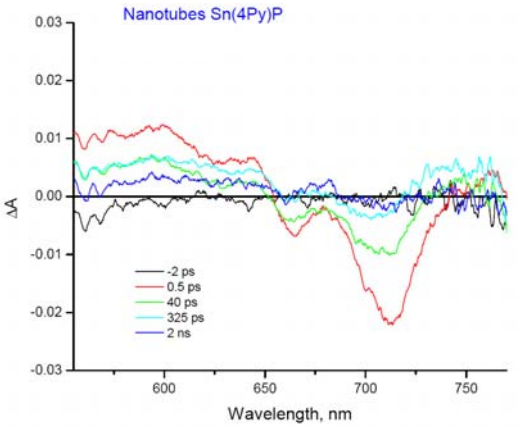

Figure 20. *Femtosecond time-resolved optical spectra of the porphyrin nanotubes.*

The colloidal nature of the platinized nanotube suspension and the intense resonance light scattering of the porphyrin nanotubes make accurately measuring the quantum yield for the formation of hydrogen difficult. Further, measurements are required to determine the quantum yields and its dependence on platinum coverage and concentration of the nanotubes. The actual conversion efficiency will depend on factors such as charge separation and recombination rates, electron diffusion lengths and rates, and other factors to be determined.

Mechanical Response to Light. Another potentially useful property of the nanotubes is their ability to respond mechanically to light illumination. Even though they are stable for at least months when stored in the dark, irradiation of a suspension of the tubes for just five minutes using incandescent light from a projector lamp (800 nmol-cm^{-2}-s^{-1}) results in TEM images showing rod-like structures instead of tubes. This response to light is partially reversible, as the tubes reform (self-heal) when left in the dark. The switch from tubular to rod-like structures in the TEM images suggests a softening of the tube walls and a collapse of the tube structure, perhaps as a result of photoinitiated intermolecular electron transfer that disrupts the charge balance and hence the rigidity of the structure of the ionic solid. Local heating from energy relaxation of the photoexcited porphyrin molecules might also explain the softening effect.

Photophysical and Electronic Properties of the Porphyrin Nanotubes. Efforts are underway to fully characterize the optical and electronic properties of the photocatalytic nanotubes. These studies may also give a better understanding of the ionic self-assembly processes. For example, femtosecond time-resolved spectroscopy of the porphyrin nanotubes with Profs Christine Kirmaier and Dewey Holten at Washington University has begun to reveal information relevant to electron and energy transport in the nanostructures. Preliminary time-resolved optical spectra of the 4-pyridylporphyrin nanotubes indicate several dynamical processes within the first 2 ns after excitation (see Fig. 20). The adaptive/responsive mechanical behavior and self-healing properties displayed by the nanotubes may provide another route toward additional information about these dynamical processes and may also lead to novel electromechanical nanodevices.

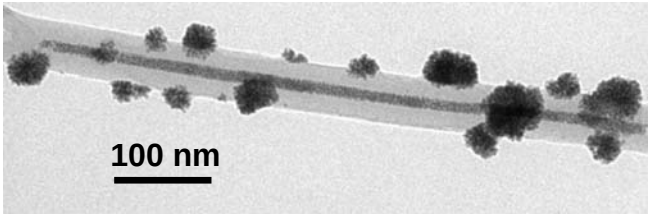

Figure 21. *A nanotube containing a dendritic Pt nanowire in its core with globular gold dendrites on the outer surface. Procedure: (a) Pt deposition: 100 µl K_2PtCl_4 solution (20 mM Pt) and 100 µl ascorbic acid solution (0.2 M) were added to a 2-ml glass vial containing 1 ml of the nanotube colloidal suspension ($SnTPyP^{2+}$ concentration 1.75 µM). The reaction mixture was swirled to homogenize the solution, placed in a glass water bath to control the temperature, and then irradiated with incandescent light (800 nmol cm^{-2} s^{-1}) for 11 min. The suspension was centrifuged at 2000 rpm for 2 min to remove the supernatant, 1 ml 0.01 M HCl was added and the mixture swirled to homogeneity. Gold deposition: 100 µl 0.2 M ascorbic acid solution and 100 µl 20 mM freshly prepared Au(I) thiourea complex solution were added and the reaction mixture was swirled again, placed in a glass water bath to control the temperature, and then irradiated with incandescent light (800 nmol cm^{-2} s^{-1}) for 9 min.*

High frequency conductivity measurements are underway at Sandia National Laboratories in collaboration with Mark Lee. AC conductivity in the microwave thru millimeter wave spectrum eliminates issues concerning the contact with electrodes applied to the nanotubes.

Molecular Control over the Structure of Porphyrin Nanotubes. By altering the molecular structure of the porphyrin tectons, the dimensions of the nanotubes can be controlled. For example, by using Sn tetra(3-pyridyl)porphyrin instead of Sn tetra(4-pyridyl)porphyrin, nanotubes (not shown) with significantly smaller average diameters were obtained (35 nm instead of 60 nm). Switching the tin porphyrins subtly repositions the charge centers and the associated H-bond donor atoms on the pyridinium rings, apparently changing the inter-porphyrin interactions sufficiently to alter the diameter while

still allowing the tubes to form. Nanotubes are not produced when the 2-pyridyl porphyrin is used however, presumably because the location of the functional nitrogen atom is changed too drastically. Axial ligation of a tecton is also important as tubes and collapsed tubes are obtained when the Sn(IV) complex is replaced with other six-coordinate metal ions (*e.g.*, Fe^{3+}, Co^{3+}, TiO^{2+}, VO^{2+}), but tubes have not been found when a metal that does not add axial ligands (*e.g.*, Cu^{2+}) or the metal free porphyrin is used. These results suggest that it may ultimately be possible to achieve a high degree of control over the structure of the tubes by modifying the tectons, including variation of the peripheral substituents of the porphyrin, the metal contained in the porphyrin core, and the nature of the axial ligands.

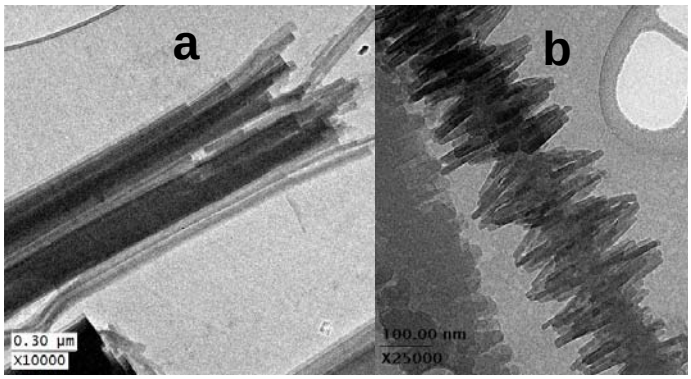

Figure 22. *Other nanostructures formed by ionic self-assembly of porphyrin tectons: (a) bundles of porphyrin nanofibers formed using a photocatalytic SbO porphyrin complex and H_2TPPS_4 as tectons and (b) firecracker-string-like nanostructures made using a photocatalytic $SnTPPS_4$ and a positively charged porphyrin as tectons.*

C. Porphyrin-nanotubes as templates for metal deposition: Toward porphyrin nanodevices

The nanotubes shown in Fig. 11 contain a photocatalytic Sn porphyrin and can reduce metal ions from aqueous solution and this metal may be selectively deposited onto the tube surfaces producing novel composite metal nanostructures.[13] The metal parts of the resulting nanostructures can serve as the conductors, interconnects, electrodes, catalytic centers, *etc*., of nanoscale devices. Nanotube-metal composites might also be made using several other metals and metal alloys. In particular, metal can be deposited selectively onto the inner and/or outer surfaces, leading to the possibility of complex hierarchical nanodevices. For example, a solar water-splitting nanodevice can be readily envisioned as a bimetallic device arising from a combination of metal component parts added to the porphyrin nanotubes. Early attempts at making nanostructures demonstrate that such bimetallic constructs can be made (see Figs. 17 and 21). We expect that variation of the porphyrin subunits in the nanostructures and of the deposited metals will ultimately produce a wide range of useful nanodevices of this type. The range of architectures that can be made suggests that the energetic and functional requirements for a wide variety of nanodevices can be met. While making such nanodevices is outside the scope of this proposal, developing the synthetic procedures and methods for controlling the formation of nanostructures composed of the porphyrin nanostructure with deposited metals is a part of the proposed work for the next award period.

D. Other porphyrin nanostructures as templates for metal deposition

It is possible to produce other porphyrin-based nanostructures besides the nanotubes by significantly altering the structure of the constituent tectons. Figs. 22 and 23 show TEM images of two other types of porphyrin nanostructures that our group has made by ionic self-assembly of porphyrin tectons. Fig. 22a shows a section of a very long bundle of porphyrin fibers. Fig. 22b shows one of the more structurally complex porphyrin nanostructures that can be made by ionic self-assembly of porphyrins, which we describe as 'firecracker strings'. We expect that other porphyrin nanostructures (see below) with a wide range of electronic properties will be found when a larger range of tectons are investigated.

One of our goals is to use these new photocatalytic porphyrin nanostructures as templates for metal growth (Fig. 23c) as was done for the porphyrin nanotubes. Again, our intention is ultimately to produce metal-composite nanostructures as nanodevices for various applications. In addition, preliminary data demonstrates that a wide range of optical properties are observed for these new porphyrin nanostructures. For example, Fig. 23a shows a confocal microscope image obtained *via* the fluorescence of the nanofibers shown in Fig. 22a. Unlike the porphyrin nanotubes, fluorescence of these porphyrin fibers is not quenched, a feature that may be desirable for certain applications. Both the nanofibers and the firecracker strings are expected to be

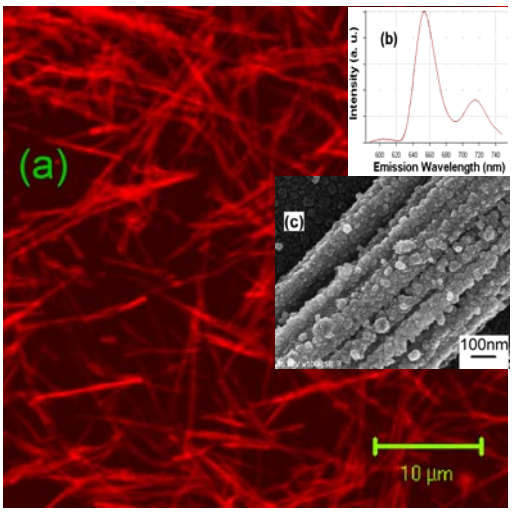

Figure 23. *(a) Conformal microscope images of porphyrin nanofiber bundle, (b)s and the fluorescence spectrum obtained from one of the fibers, and (c) platinum grown on the fibers.*

photocatalytically active because one of the pair of porphyrin tectons in each case is a photocatalytic tin or antimony porphyrin complex. For the nanofibers, the photocatalytic activity has been used to grow platinum (Fig. 23c) and gold (not shown) onto the fiber bundles. We will focus our future work in this area on making photocatalytic porphyrin nanostructures and metal constructs derived from them. This will provide a rich area of research, partly because of the myriad nanostructures that can be made using ionic self-assembly, and partly because of the demonstrated ability of some of these nanostructure to be selectively coated with metals.

Much remains to be learned about the structure and function of the porphyrin nanostructures, how they form by self-assembly, what causes the remarkable surface selectivity for metal deposition, and how to exploit their inherent photocatalytic and other functional properties to make functioning nanodevices.

4.3 Research Design and Methods

A. Nanoengineered metals and metal nanostructures.

Now that we have obtained a better understanding of the role of photocatalysis in the platinum reduction reaction and characterized several Pt nanostructures, we will focus on exploiting this new understanding to make novel nanomaterials. Several new opportunities for creating unique functional nanostructures are evident and will be pursued in the next contract period. Similarly, now that we have begun to characterize the properties of these nanomaterials, we can begin to focus on learning how to modify the properties of these materials for use in various applications.

One of our near term goals is to fabricate fuel cell electrocatalysts based on the materials that have already been made and test these in membrane electrode assemblies. Indeed, we have shown that the platinum foams have a high surface area, comparable to that of the commercial fuel-cell grade platinum black (5-6 nm particles), and possibly even better electro-active surface areas. Moreover, the foams are composed of interwoven circular dendritic nanosheets possessing a diameter up to several hundred nanometers, and this morphology may provide better conductivity than Pt nanoparticles supported on other conducting materials. The self-supporting nature of the foams may allow us to avoid using supporting conductors, thus reducing the thickness of the catalyst layer of the membrane electrode assembly (MEA) in proton exchange membrane (PEM) fuel cells while maintaining good mass transport characteristics. Thin catalyst layers are though to be important[21] as shown by data for PEM fuel cells composed of a thin MEA with 10-12 nm platinum nanoparticles deposited on organic whiskers without using carbon support. The thin catalyst layers can provide a higher heat and water generation rate per unit volume and a higher efficiency of the catalyst at all current densities. In addition, a shorter electrode ionic resistive path results because the protons have less distance to percolate between the PEM and the reacting catalyst surface sites compared to the conventional thick catalyst layer using 3-5 nm platinum particles supported on carbon. Macropores formed by the liposome void space existing among the randomly packed individual spherical foam balls and nanoscale crevices existing between the dendritic arms of the Pt sheet will facilitate the mass transportation in the fuel cell applications. This property of the foams is similar to the case in which bigger 10-12-nm particles on organic polymer whiskers are used, and these fuel cells generate a higher current density than when 3-5 nm particles on carbon are used. Although still controversial, another factor that may provide higher activity for the Pt whiskers and our nanofoams is the increased effective size of the platinum nanoparticles, which may contribute to the higher current density by providing a more bulk-metal-like (higher) Pt catalytic activity. Since the metal is highly extended in the plane of the Pt sheets of the foams, bulk-like activity potentially can result, giving higher catalytic activity in our high surface area, conductive nanostructures, and this could generate PEM fuel cells capable of operating at high current densities. The tasks then are to build the MEA, optimize the operating conditions (such as air and hydrogen flow rates, humidity, platinum loadings, membrane materials and their combination), and measure MEA performance

We will also focus part of our efforts on making new nanomaterials that are versions of the platinum foam structures with improved catalytic properties. In particular, reduction of platinum content is a strategic goal of fuel cell research, and we are thus pursuing other types of metallized liposomal nanostructure including liposomes coated with dendritic palladium, gold, and Pd/Au alloys. In this funding period, we will also turn our attention to other metals (M = Au, Cu, Ag, Pd, Re, Ni, Fe, Co, Zn) and alloys of these metals to demonstrate that our original idea of pre-positioning the porphyrin photocatalyst and then growing metals at the location of the photocatalyst molecules can be generalized. Tasks here are to prepare alternative catalysts, such as PtM alloy, PdM alloy or ReM alloy that reduce the platinum content using the porphyrin photocatalysis method. These platinum-metal alloy foams will be used in catalytic hydrogenation reactions, in fuel cell electrodes, and as oxidation catalysts in the production of acetic acid, nitric acid from ammonia, and in automotive emissions control reactions. Characterization of the

catalysts will be done using TEM, STEM, SEM, XRD, DTA-TGA, N_2 adsorption-desorption, electrochemical measurements, and gas chromatography will be employed to quantify products and obtain reaction rates.

We will also investigate the possibility of growing both the pure metals and alloys as dendrites on other types of supports besides surfactants. For example, a DSPC/cholesterol bilayer containing tin porphyrin photocatalyst can be deposited on a flat surface, such as silicon and mica, by LB film techniques. Then, dendritic metal and semiconductor dendritic nanosheets can be grown photocatalytically on these flat substrates as a way of doing controlled studies of the growth processes as well as producing new materials. These modified substrates have potential applications as electrodes and sensors. Similarly, growth of dendritic metals in the interfacial region between a surfactant layer and the surface of a porous support might provide novel catalysts and electrocatalyst for a variety of applications. We will try to grow metals on high surface area polymer substrates as a test case.

We will search for other templating structures and methods for localization of the photocatalyst molecules. Some strategies to be studied are: (1) to embed the porphyrin in self-assembled 1,2-bis(10,12-tricosadiynoyl)-*sn*-glycero-3-phosphatidylcholine (DCPC) lipid nanotubes, (2) to extrude liposomes containing the porphyrin through porous alumina membranes to coat the channels with lipid bilayer containing the photocatalyst, which can then be used as hybrid templates to direct the growth of metals and semiconductors into nanotube arrays, (3) to localize the porphyrin in lyotropic mixed surfactants (*e.g.*, $C_{12}EO_9$ and Tween 20-60) that from liquid crystals in order to synthesize photocatalytically controlled nanostructure arrays, and (4) to modify peptide nanotubes with surface-attached porphyrins that can be used to metallize the tubes.

Another synthetic approach is use the interface between bulk organic solvent and water phases to template formation of metal nanostructures as illustrated by the nano- and microscale emulsion experiments illustrated in Fig. 16. Since the tin-porphyrin photocatalyst is most soluble in water, while its hydrocarbon tails are readily soluble in the organic phase, the porphyrin headgroup is trapped at the interface. The metal precursor and the electron donor are both highly soluble in water so the metal reduction must take place mainly at the organic/aqueous interface. In preliminary experiments, we have found that metal reduction at the interface results in a thin shell of metal deposited on the interface as in Fig. 16. In the case of gold, growth at the interface between a layer of organic solvent and an overlying aqueous layer results in the formation of planar sheet-like gold particles or nano-plates of large aspect ratio. These are typically triangular nanoplates with edge lengths of ~300 nm and thickness of ~30 nm (not shown). For this reaction, the photocatalyst was dissolved in benzene while the gold precursor, $HAuClO_4$ and citric acid (ED) were dissolved in water. With higher acidity for the aqueous phase, triangular or hexagonal Au nanosheets with dimensions up to a few microns and thickness of ~30 nm have been prepared. We expect that the Au nanoplates will have applications in single-molecule detection by surface enhanced Raman spectroscopy. We will continue to explore this new approach to forming metal nanostructures in the next funding period.

B. Porphyrin nanostructures and their metal and semiconductor nanocomposites

Structural characterization of the porphyrin nanotubes. Although the structure of the porphyrin nanotubes is well characterized by electron microscopy, the detailed packing of the porphyrin molecules in the tubes is at present poorly defined. High resolution TEM images of tubes in an end-on orientation show that the tubes have a lamellar structure, with the spacing of the lamellae of 1.7 to 1.8 Å. The variation in the wall thickness appears to be a consequence of different numbers of lamellae. The dark bands of the TEM images are probably indicative of the location of the heavy Sn and S atoms of the two porphyrins. One method we will use to obtain additional information about the packing and relative positions of the two types of porphyrins in the tubes will be to label the porphyrins with heavy atoms (e.g., Br) at specific positions and to examine the resulting high resolution TEM images. High resolution scanning tunneling microscopy (STM) will also be performed in collaboration with Prof Ursula Mazur at Washington State University. Preliminary STM images obtain in Prof. Mazur's lab (Fig. 24) may ultimately provide detailed structural and functional information on the porphyrin nanotubes. UV-visible absorption, resonance light scattering, resonance Raman, and NMR spectroscopy at Sandia will also be brought to bear on this problem to obtain information about the arrangement of the porphyrins in the tubes.

Characterization of the electron- and energy-transport properties of the porphyrin nanotubes and their metal-composite structures. Our primary method for characterizing electron and energy transport will be femtosecond time-resolved absorption and emission spectroscopy, which will be carried out in collaboration with Prof. Christine Kirmaier at Washington University. Christine Kirmaier and Dewey Holten are the leading experts in the excited state dynamics of porphyrins and porphyrin arrays,[22-25] and they have also done much of the work on time-resolved spectroscopy of the photosynthetic proteins, especially studies of reaction centers.[26-29] Most recently, Holten and Kirmaier have been investigating self-assembling arrays of porphyrins as light-harvesting arrays[30] as are other researchers.[29]

We have recently obtained the first time-resolved spectroscopic results on the porphyrin nanotubes. Fig. 20 shows a region of the spectrum of the nanotubes containing one of the *J*-aggregate bands. Bleaching of the band is observed as well as formation of additional species in the first 2 ns of evolution of the spectrum. These excited state species will be identified and their formation and decay rates determined, and similar data will be obtained for bands evident in other regions of the time-resolved spectra.

Excitation energy hopping (EEH) processes have been observed within other systems of porphyrins using femtosecond time-resolved absorption and fluorescence. It is thought that regular cyclic arrangement and large electronic couplings between neighboring pigments are required for efficient EEH. We expect that the strong electronic coupling and circular arrangements of the porphyrins in our nanotubes may satisfy these requirements for efficient EEH. There are currently good models available for the EEH processes involved in biological light-harvesting systems.[31, 32] These models describe Forster-type incoherent exciton migration and include fast decay mechanisms associated with exciton-exciton annihilation. We will measure the time-resolved absorption and time-resolved absorption anisotropy decays and then we will employ the current computational models to determine the EEH rates for the nanotubes. We have noted the marked quenching of the fluorescence of the monomeric porphyrins when in the nanotubes, but the fluorescence may be sufficient to measure ultrafast fluorescence depolarization decay. However, the nanotubes are more complex than the light-harvesting proteins in that two types of porphyrins are involved and they most likely have a lamellar structure, and not just rings of pigments as in the light-harvesting complexes. In addition, there likely is energy transfer between multiple lamellae to consider. We also expect electron as well as exciton hopping to be in evidence within the porphyrin aggregates, especially in the presence of sacrificial electron donors and in the functional water-splitting nanodevices. Thus, it is likely that current models will be insufficient to describe the photophysical process occurring in the nanotubes, and new models may have to be devised to aid in interpretation of the time-resolved spectroscopic data. We will focus our studies on understanding EEH and electron transfer processes in the nanotubes, their metal and semiconductor composites, and other porphyrin nanostructures.

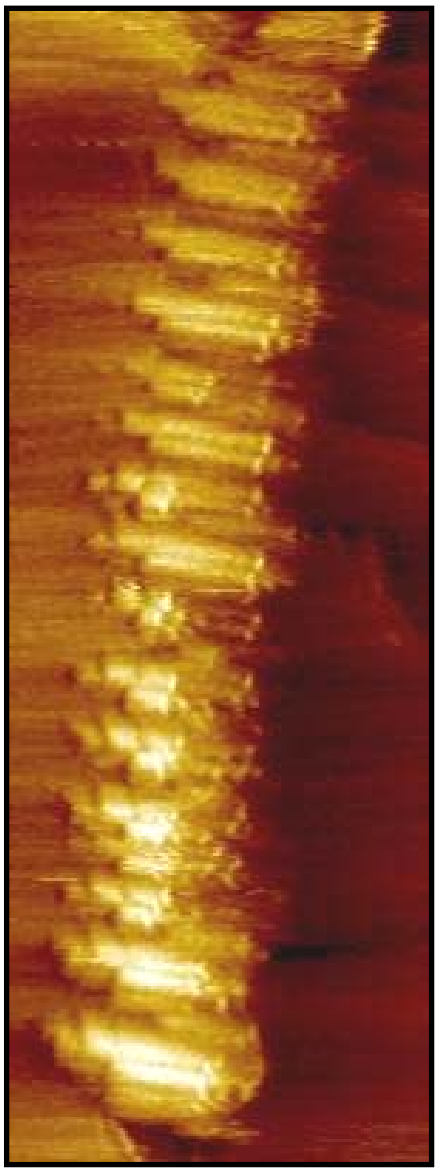

Figure 24. *STM 100-nm wide image of TPPS-SnT(4Py)P tubes on iodine modified Au(111). Bias voltage -0.800 V. Sample was dried under vacuum for several hours prior to imaging.*

The conductive properties of these nanotubes will be measured using a number of conductive AFM techniques in collaboration with Dr. Kevin Zavidil at Sandia National Laboratories. AC electrical conductivity measurements are already underway at Sandia in collaboration with Mark Lee. Variant techniques like scanning gate and impedance microscopies rely on potential induced current measurements to measure DC and AC conductivity along the nanotube. These techniques have been used previously to investigate carbon nanotube properties. The low currents intrinsic to nanodevices make AC techniques particularly attractive given the benefit of intrinsic noise reduction due to synchronous modulation. Attaching nanodevices to electrode surfaces coupled with the availability of micro- and nano-scale interdigitated electrode arrays will allow for a full characterization of anisotropic conductivity for these nanotubes and nanodevices. We will also investigate the possibility of functionalizing cantilever tips with nanotubes to study the axial conductivity. We will be focused on understanding the structure-property relationships that control the conductivity of the tube under dark and illuminated conditions.

We will expand our characterization and imaging to *in situ* environments. Here we take advantage of our electrochemical AFM capability and build upon what we learn with regard to tube synthesis, attachment and conductivity properties. The goal is to determine how interfacial electron transfer efficiency is distributed along the length of the nanotube as well as its relationship to metal particle size and dispersion on the tube surface. A number of possibilities exist for making this measurement including highly localized potential measurements based on H^+ activity, scanning electrochemical microscopy (SECM) based on H_2 oxidation at a scanned tip, or H^+ mediated

chemistry that relies on diffusional blocking of a SECM probe. While spatial resolution is not extremely high for these solution techniques, it may be sufficient to investigate variation along the tube length. No other techniques currently exist that allow this level of chemical and spatial fidelity. These techniques are equally suitable for characterizing the activity of structures fabricated from ensembles of nanotubes and other porphyrin nanostructures.

Eventually, we want to understand factors determining the ability electrons in the conduction band of the porphyrin nanotubes to migrate to the platinum nanoparticles on the surfaces of the tubes, with a view toward using as little of this precious metal as possible in functional devices such as solar water-splitting nanodevices. If the electron transfer within the porphyrin nanotubes is fast and efficient, it is likely that no more than a few Pt nanoparticles per nanodevice would give optimum function for formation of hydrogen from water. It is also likely that the surface of the nanotubes might ultimately be modified with attached biomimetic proton-reducing catalysts or hydrogenase itself to completely eliminate the need for Pt metal.

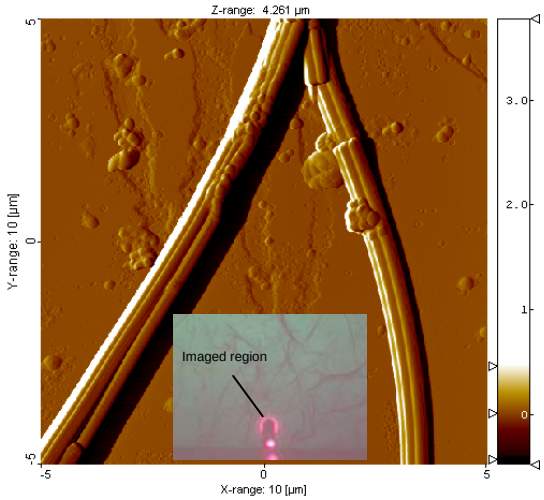

Figure 25. *Topography AFM amplitude image of bundles of porphyrin nanofibers obtained using the tapping mode of operation. Inset: Optical image showing the region imaged by AFM. Individual fibers of the bundles are approximately 27 nm in diameter.*

Synthesis of new photocatalytic porphyrin nanostructures as metal-growth templates. Synthetic methods for producing additional photocatalytic porphyrin nanostructures besides the nanotubes, such as fibers, wires, *etc.* will be explored. As part of our near-term goals, new tube-forming porphyrin tectons will be examined in order to generate photocatalytic nanotubes with different diameters, lengths, wall thicknesses and altered photocatalytic properties. We previously described some preliminary results in this area; in particular, we showed that changing the 4-pyridyl group to a 3-pyridyl group decreased the diameter of the porphyrin nanotubes, while changing to the 2-pyridyl substituent group apparently does not allow tube formation. Given the large number of synthetic methods for structurally modifying porphyrins, and the expertise of Dr. Craig Medforth in porphyrin synthesis, we will have access to a significant library of potential porphyrin tectons. As an example, we intend to investigate the tin complex with a 4-aniline group rather than the 4-pyridyl group of the porphyrin shown in Fig. 12. This could potentially increase the intermolecular H-bonding between the tectons, thereby producing sturdier nanotubes. Another possibility is to alter the metal in the core of the porphyrin to another that is photocatalytically active such as Sb(V), thereby altering the redox properties and photocatalytic states and lifetimes of the nanotubes. Studies of this type will allow us to gain insights into the role of tecton-tecton interactions in producing a particular nanostructure, which is poorly understood at present. They should also shed light on the details of the ionic self-assembly process used to make the porphyrin nanostructures, and how the constituent porphyrins of the nanotube affect the self-metallization reactions of the tubes. The metallization reactions of the new nanotubes developed in this manner will also be investigated, especially as regards the metal-complex and water reduction reactions.

Besides the nanotubes, the bundles of fibers shown in Figs. 22a and 23 are also of interest because they self-assemble in organic solvent, so they can be handled and processed in different ways from the nanotubes that are formed in an aqueous environment. In addition, preliminary examination of the optical spectra of these nanofibers (and the firecracker strings) shows that their electronic and optical properties are quite different from those of the nanotubes. For example, whereas the porphyrin nanotubes show intense resonance light scattering consistent

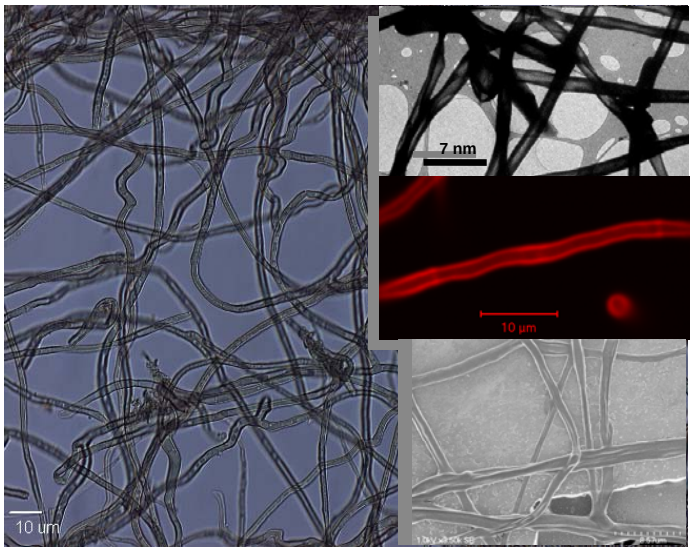

Figure 26. *Optical microscope image of three-component porphyrin microtubes formed by ionic self-assembly. Insets (top to bottom): TEM image, confocal fluorescence image, SEM image.*

with the formation of *J*-aggregates, the fibers and firecracker strings lack significant resonance light scattering. This indicates a different kind of interaction between the porphyrins in the fibers and firecracker strings compared to the nanotubes, and differences in the electronic coupling of the porphyrin subunits. Being able to vary both the catalytic, electronic, and optical properties as well as the morphology of the porphyrin-based nanostructure is a highly desirable feature of our porphyrin-based nanostructures.

Representative AFM images of the nanofibers shown in Figs. 22 and 23 are given in Fig. 25. The image of the nanofibers on mica was generated in intermittent contact ("tapping") mode in air using a Si cantilever with a tip curvature radius of less than 10 nm and a full tip cone angle of 30°. Individual nanofibers are readily imaged in AFM. Images of the smallest features that are optically visible on the AFM system, such as some of the very fine fibers that show up in the optical micrograph shown in the Inset in Fig. 25, show that the nanofibers are bundles of smaller diameter fibers with their axes aligned parallel to that of the bundle. The image shows two fiber assemblies with composite diameters of 550 and 150 nm for the left and right bundles, respectively. The diameter of an individual fiber within one of these bundles is estimated at 27 nm by measuring the step height across the smaller bundle. This diameter measurement for fibers is in good agreement with the diameter for the individual fibers obtained from TEM images.

Figure 27. *SEM image of porphyrin 'clover' formed by ionic self-assembly of two oppositely charged porphyrins. Upper Inset: TEM image. Lower Inset: Confocal image, showing preferential fluorescence from spines of the clover leaves.*

Very recently, we have discovered additional types of porphyrin nanostructures that may be of interests as catalysts. Fig. 26 shows very long microscale tubes composed of two porphyrins and an amino acid. Although these tubes are very flexible and have thin walls, they can be millimeters long suggesting good tensile strength. Fig. 26 shows optical, fluorescence, SEM, and TEM images of these new porphyrin microtubes. The composition of these tubes has not been fully characterized, but they are most likely chiral because of the incorporated L-amino acid. We will characterize their catalytic properties, including the expected photocatalytic activity induced by the tin-porphyrin component of the tubes.

Another very recently discovered example is the porphyrin 'clover' shown in Fig. 27. Most of the porphyrin ionic solid is in the form of these macroscale four-leaf structures; some features of the clovers are nanoscale. The confocal microscope images of the emitted light (fluorescence) suggest the certain regions of the clovers (*e.g.*, the spines of the leaves) preferentially emit light while for other parts (*e.g.*, the central column) the emission is suppressed. (See Inset of Fig. 27.) The fluorescence emission may also be directional. It will be interesting to photocatalytically deposit metal onto the clover, since electron transport to the surfaces may also be spatially selective.

Metal- and semiconductor-composite superstructures. We will first explore synthetic strategies for selectively depositing metals at various locations on the nanostructures (*e.g.*, inside/outside, edges/flat surfaces, etc.). For example, one task will be to develop synthetic strategies for attaching metal-oxide semiconductor nanoparticles and organic materials directly to the porphyrin nanostructures. It will be useful to develop such synthetic methods with the ultimate goal of making complex, multi-component nanostructures for coupled photo-redox and other catalytic reactions. Coupling of catalysts at the nanoscale may lead to novel catalytic and photosynthetic reactions. We will investigate coupling of the nanotubes and other porphyrin nanostructures to both inorganic and organic species.

Metal oxide nanoparticles could be attached simply by adsorption onto deposited metal surfaces or through organic linker molecules (*e.g.*, a thiol-functionalization of the surface of a metal oxide for linking to deposited gold on the porphyrin nanostructure). Another possibility is to connect the metal oxide linker molecule directly (covalently) to the porphyrins of the nanostructure. Preferably, we would be able to spatially direct the linker to a specific location on the nanostructure (*e.g.*, the core or outer surface of the nanotubes). These synthetic methods could also be used to connect the nanostructures directly to electrodes to catalyze electrochemical reactions. Such self-organized nanoscale superstructures, composed of the porphyrin nanostructure and attached metal, inorganic, and organic components, will ultimately lead to nanodevices desirable for catalytic, photocatalytic, and electrocatalytic reactions.

Modeling the structure and properties of porphyrin nanostructures and nanodevices. At present we have only a limited understanding of the internal structure of the porphyrin nanotubes and other porphyrin nanostructures.

Optical studies of the tubes suggest a J-aggregate structure for the porphyrin subunits and TEM images show fringing consistent with a lamellar structure of these aggregates. We plan to use theory and simulation to improve our understanding of the structures of the nanotubes and other porphyrin-based nanostructures such as those shown in Figs. 22, 23, 25-27. The theoretical methods available to us should permit us to accurately model the structure and dynamical behavior of these complex systems over a range of time and length scales, providing the understanding required to discover and exploit new nanoscale phenomena in these supramolecular assemblies.

Given the size of these systems, an obvious first step in modeling the nanostructures is to use molecular mechanics calculations to investigate the local interactions of small numbers of porphyrin tectons to help determine how they assemble. This effort will be aided by an in-house molecular mechanics force-field, which we have developed over the last decade.[33-47] This force-field can accurately reproduce the crystal structures of porphyrins, even highly distorted ones, and has also been proved capable of predicting the dynamic properties of porphyrins such as substituent rotation and ligand rotation. The molecular mechanics calculations can give us a better understanding of the local interactions between the porphyrin tectons and thus the internal structures of the nanomaterials, which will help us to design new systems with specific structural and functional properties.

The second goal of our modeling effort is to understand the relationship between the structure of the porphyrin tectons and the shape and size of the assembled nanostructure. This is a challenging goal that may be reached with the aid of advanced computational methods, including Monte Carlo (MC) molecular dynamics (MD) and Classical Density Functional Theory (CDFT). In collaboration with Prof. Frank van Swol, we recently have used Monte Carlo simulation to investigate the self-assembly of the dipeptide D-Phe-D-Phe into peptide nanotubes.[48] In the study of the peptide nanotubes, a simplified structure of the dipeptide was used in lattice-MC simulations performed using a lattice model with periodic boundary conditions. The model reproduced tubular structures and defined the orientations of the individual dipeptides. The model also gave a possible explanation for the apparent porosity of the tube walls by suggesting that the walls might consist of a porous bicontinuous phase. We plan to investigate a similar computational approach for studying the self-assembly of the porphyrin nanostructures from their component tectons.

We plan to build our initial efforts on simple models that account for ion shape and size and the competition between positive and negative charges derived from the molecular mechanics calculations. This is a natural starting point. We know from simulations of related simple ionic crystals (*i.e.*, salts such as alkali halides) that the crystalline structure can be entirely understood on the basis of the charge ordering that reflects the interplay between like and unlike ions and ionic size. That is, neither the long-range of the electrostatic interactions nor their precise nature is crucial to the assembly of ionic crystals. Even models that represent the like and unlike interactions by finite-ranged r^{-5} potentials, say, will give rise to radial distribution functions that are very close to those of actual infinitely-ranged r^{-1} interactions. In fact, our recent MD simulations clearly demonstrate that even a non-additive binary hard sphere model (infinitely short-ranged) faithfully reproduces the variety of observed ionic structures and also explains the known reduction in melting point temperature with ion size (which can be very dramatic in the case of so-called ionic liquids).

Once a porphyrin structure has been found (or proposed) CDFT can be used to determine the charge distribution. This is done by defining the location of charge centers and minimizing the grand potential with respect to the spatial distributions of positive and negative charge distributions. The minimization is performed subject to the constraints of electro-neutrality and the total positive and total negative charge. This approach can be applied to the interior of the tube wall as well as the inner and outer surfaces.

The experimental evidence suggests that the two types of porphyrins that form the tubes do so by a process of ionic self-assembly. In essence, the porphyrins, which carry (partial) charges on the metal and the peripheral substituent groups in solution, assemble by stacking in a particular order by excluding volume and by minimizing the free energy that is dominated by electrostatic and excluded volume contributions of the tectons. Such self-assembly would be equivalent to the simpler one seen for the formation of a crystal from a NaCl solution, or the freezing of an ionic liquid. In both these cases, the crystal lattice that is observed (*e.g.*, rock salt *versus* zinc blende, say) is known to depend on ionic size and the electrostatic charge. The porphyrins are more complex than the examples cited in the sense that besides carrying

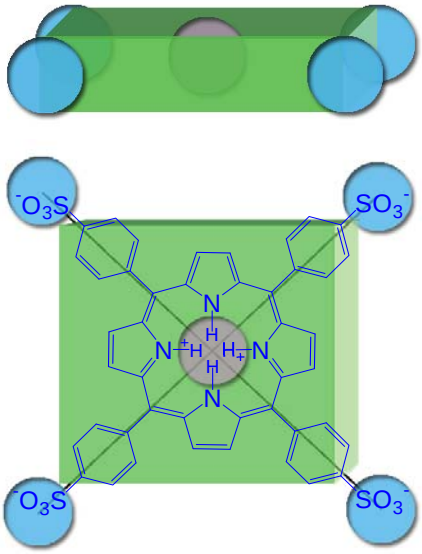

Figure 28. *Two schematic views of a model porphyrin tecton consisting of a parallelepiped (green) and five spherical charge centers (blue-negative, pink-positive). The bottom half provides the top view, which highlights the flexible position of the charge centers relative to the parallelepiped.*

a net charge, the porphyrin tecton can, and in our case does, support opposite charges on the same tecton. Whereas the self-assembly of the simple salts such as NaCl and KBr formed by combining ionic versions of the elements of the periodic table is of course well-studied, the understanding of ionic assembly of so-called ionic liquids is still in its infancy. The reason for this is simply that the effect of excluded volume contribution for large non-spherical organic ions is much more difficult to predict and account for in calculations than that of the familiar spherical elemental ions.

To start building a fundamental understanding of the ionic assembly process of porphyrins into tubes and other nanostructures we propose to use Monte Carlo simulations of a highly simplified model. This is the natural place to start as the multi-charge non-spherical porphyrin ions constitute an entirely new class of materials about which little is known. In addition, our recent experience with ionic liquids[49] demonstrates that very simplified models (such as non-additive hard spheres) are capable of capturing the salient features of ionic self-assembly.

We will capture the shape and excluded volume of our porphyrins by representing each tecton by a hard parallelepiped decorated with four charge centers near the periphery and one charge center located at the parallelepiped's center of mass. The peripheral charges are located in a plane that bisects the parallelepiped (see Fig. 28). The detailed position of the corner spheres relative to the edge of the parallelepiped can be varied to provide further model flexibility. The interaction between the two types of charge centers on different tectons consists of a short-ranged repulsion (providing the excluded volume between charge centers) plus an electrostatic contribution that is positive for unlike charges and negative for like charges.

Simulations will be run for binary mixtures of two such tectons, with the composition and partial charges chosen such that the overall system is electrically neutral. Initially, values for the partial charges will be taken from experiments, but we will also consider a theoretical route (*i.e.*, using DFT calculations). Following the strategy for ionic liquids[49], we will start from a dilute state and will employ NpT Monte Carlo to slowly compress the system to densities where we can expect ordering to take place. In this regime various traversals will be made (by varying the density) looking for signs of a spontaneous phase transition (monitoring order-parameters and changes of slope in the p-V isotherms). Free energy calculations will be used to determine the relative stability of various solid phases (*i.e.*, various stacking arrangements), including those that may arise from the spontaneous order simulations. Once stable ordered structures have been identified we will consider large scale simulations to determine the possibilty of calculating the observed tubular structures.

A tantalizing long-term goal of such studies would be the ability to predict the structure(s) formed by specific combinations of tectons using only computational methods. The calculations might obviate the need for some tecton synthesis, assembly, and imaging in the laboratory. In such a case, the discovery of new porphyrin-based nanostructures would be limited only by the computational power and synthetic capabilities at our disposal.

CDFT will also be used to obtain the structure of the double layer, both inside the tube and outside. Knowing the structure of the double layer, and hence the electrostatic potential inside and outside the tube, is considered crucial in helping build an understanding of the growth of metal nanostructures on porphyrin nanotube surfaces as well as the functioning of the proposed nanodevices. In particular, knowing the electrostatic potential field is expected to help explain why positively charged metal complexes lead to metal growth inside the tube while negatively charged complexes promote metal growth on the outside.

Theoretical methods can also be used to investigate the electronic properties of the porphyrin nanostructures. Recently, we completed a comprehensive study of the effects of nonplanarity on the optical properties of porphyrins using our molecular mechanics force-field in combination with semi-empirical (INDO) calculations.[46] INDO calculations could be used in a similar fashion to simulate the optical spectra of the nanostructures and the aggregates that they contain. In this way, the optical spectra calculated for different proposed structures could be compared to the experimentally observed spectra, allowing us to determine whether the proposed structure is reasonable. We are currently developing and evaluating the use of time-dependent density functional theory, using the Amsterdam code (ADF), as an improvement over the INDO/S methods that have typically been used by our group.

The electron and energy transfer rates might also be inferred from various molecular models and compared to those observed experimentally. This will provide a means of assimilating, testing, and refining the proposed electron- and energy-transfer mechanisms of some of the more complex composite nanostructures and will supply new strategies for optimizing catalytic rates.

References of Publications that Acknowledged the Previous Grant:

Journal articles:

1. "Porphyrin nanotubes by ionic self-assembly" Wang, Z.; Medforth, C. J.; Shelnutt, J. A., *J. Am. Chem. Soc.* **2004**, *126*, 15954-15955.
2. "Self-Metallation of Photocatalytic Porphyrin Nanotubes" Wang, Z.; Medforth, C. J.; Shelnutt, J. A., *J. Am. Chem. Soc.* **2004**, *126*, 16720-16721.
3. "Controlled synthesis of 2-D and 3-D dendritic platinum nanostructures" Song, Y.; Yang, Y.; Medforth, C. J.; Pereira, E.; Singh,A. K.; Xu, H.; Jiang, Y.; Brinker, C. J.; van Swol, F.; Shelnutt, J. A., *J. Am. Chem. Soc.* **2004**, *126*, 637-645.
4. "Synthesis of peptide-nanotube platinum-nanoparticle composites, Song, Y.; Challa, S. R.; Medforth, C. J.; Qiu, Y.; Watt, R. K.; Pena, D. A.; Miller, J. E.; van Swol, F.; Shelnutt, J. A., *Chem. Commun.* **2004**, 1044-1045.
5. "Energetics and structural consequences of axial ligand coordination in nonplanar nickel porphyrins" Song, Y.; Haddad, R. E.; Jia, S.-L.; Hok, S.; Olmstead, M. M.; Nurco, D. J.; Schore, N. E.; Zhang, J.; Ma, J.-G.; Smith, K. M.; Gazeau, S.; Pécaut, J.; Marchon, J.-C.; Medforth, C. J.; Shelnutt, J. A., *J. Am. Chem. Soc.* **2005**, *127*, 1179-1192.
6. "Platinum Dendrites" Song, Y.; Shelnutt, J. A., *Nanotechnology* **2005**, submitted.
7. "Photocatalytically Nanoengineered Foam-Like Platinum Materials Templated on Liposomes" Song, Y.; Singh, A. K.; Wang, Z.; Qiu, Y.; Shelnutt, J. A., *Angew. Chem., Int. Ed. Engl.* **2005**, submitted.
8. "Porphyrin nanofibers by phase-transfer induced ionic self-assembly" Wang, Z.; Medforth, C. J.; Shelnutt, J. A. *J. Am. Chem. Soc.* **2005** in preparation.

Patents and patent disclosures:

1. "Dendritic Metal Nanostructures" Song, Y.; Pereira, E.; Medforth, C. J.; Shelnutt, J. A., Patent Application filed: 07-2004.
2. "Heteroporphyrin Nanotubes and Composites" Wang, Z.; Medforth, C. J.; Shelnutt, J. A., Patent Application filed: 12-2004.

Selected Conference Proceedings and Non-Reviewed Documents:

1. "Controlled Synthesis of 2-D and 3-D Platinum Dendrites Using Porphyrin Photocatalysts" Yujiang Song, Yi Yang, Craig J. Medforth, Eulalia Pereira, Anup K. Singh, Huifang Xu, Yingbing Jiang, C. Jeffrey Brinker, Frank van Swol, and John A. Shelnutt, American Chemical Society Annual Meeting, New York, NY, Sept 6-11, 2003.
2. "Synthesis and Control of Globular Platinum-Particle Nanoassemblies" Yujiang Song, Xiaolin Lu, Yi Yang, Craig J. Medforth, Frank van Swol, John A. Shelnutt, Materials Research Society, Spring Meeting, Apr 21-25, 2003
3. "Controlled Photocatalytic Growth of Platinized-Micelle Nanostructures" Yi Yang, Eulalia Pereira, Yujiang Song, Craig J. Medforth, Frank van Swol, C. Jeffrey Brinker, John A. Shelnutt, Materials Research Society Spring Meeting, Apr 21-25, 2003.
4. NGWA Conference on MTBE and Perchlorate: Assessment, Remediation, and Public Policy; 05/26/05; San Francisco, CA Anderson, W.L., Nuttal, E.H., Studer, J.E., Shelnutt, J.A., 2005
5. "Self-assembly of peptide nanotubes as templates for the formation of bionanocomposites" Song, Y.J.; Challa, S.R.; Shelnutt, J.A.; van Swol, F.B., Rio Grande Symposium on Advanced Materials, Albuquerque, NM, 10/25/2004.

6. “Porphyrin Nanotubes by Ionic Self-Assembly”, Medforth, C.J.; Wang, Z.; Shelnutt, J.A. National American Chemical Society meeting; San Diego, CA, 03/13/2005.
7. ”Porphyrin Nanotubes by ionic self-assembly” Medforth, C.J.; Wang, Z.; Shelnutt, J.A. Sixteenth Annual Rio Grande Symposium on Advanced Materials, Albuquerque, NM, 10/25/2004.
8. “Mimicking Photosynthesis to make functional Nanostructures and Nanodevices” Shelnutt, J.A.; Medforth, C.J.; Pereira, E.; Song, Y.; Wang, Z., Spring Materials Research Society Meeting, San Francisco, CA, 03/28/2005.
9. “Mimicking Photosynthesis to make functional Nanostructures and Nanodevices” Shelnutt, J.A.; Medforth, C.J.; Pereira, E.; Song, Y.; Wang, Z.; Nanotech 2005, Anaheim, CA, 05/28/2005.
10. “Mimicking Photosynthesis to make functional Nanostructures and Nanodevices” Shelnutt, J.A.; Wang, Z.; Medforth, C.J.; Pereira, E.; Qiu, Y.; Song, Y.; van Swol, F.B., NanoElectronics & Photonics Forum, Palo Alto, CA, 10/25/2004.
11. “Growth of Metal and Semiconductor Nanostructures Using Localized Photocatalysts” Shelnutt, J.A. 2005 DOE/BES Catalysis Program Contractor’s Meeting, Rockville, MD, 05/18/2005.
12. “Dendritic Platinum Nanostructures” Pena, D.A.; Miller, J.E.; Pincus, J.L.; Sasaki, D.Y,; Shelnutt, J.A.; Song, Y.; Steen, W.A., Spring Materials Research Society Meeting, San Francisco, CA, 03/28/2005.
13. “Mimicking Photosynthesis to make Nanodevices from Porphyrin Nanostructures” Shelnutt, J.A.; Medforth, C.J.; Pereira, E.; Song, Y.; Wang, Z., SRI, International and Silicon Valley NanoVentures, Menlo Park, CA, 03/28/2005.
14. “Mimicking Photosynthesis to make functional Nanostructures” Shelnutt, J.A.; Medforth, C.J.; Pereira, E.; Qiu, Y.; Song, Y.; Wang, Z.; van Swol, F.B.; Department of Chemistry, Washington State University, Pullman, WA, 10/03/2004.
15. “Mimicking Photosynthesis To Make Functional Nanostructures and Nanodevices” Shelnutt, J.A.; Medforth, C.J.; Pereira, E.; Song, Y.; Wang, Z., NanoTech2005, Anaheim, CA, 05/08/2005.
16. “Platinum Dendrite Nanostructures for Fuel Cells” Pena, D.; Song, Y.; Miller, J. E.; Shelnutt, J. A., 19th Annual Symposium of the Western States Catalysis Club, Albuquerque, NM, 02/25/2005.
17. “Mimicking Photosynthesis to Make Functional Nanostructures” Medforth, C. J.; Wang, Z.; Song, Y.; Shelnutt, J. A., 228th National American Chemical Society meeting, Philadelphia, PA, 08/22-26/2004.
18. “Hetero-porphyrin nanotubes and nanorods” Wang, Z.; Shelnutt, J. A., 3rd International Conference on Porphyrins and Phthalocyanines, New Orleans, LA, 7/13/2004.
19. “Controlled synthesis of lace-like platinum nanostructures using a porphyrin photocatalyst” Song, Y.; Qiu, Y.; Singh, A.; Shelnutt, J. A., 3rd International Conference on Porphyrins and Phthalocyanines, New Orleans, LA, 7/11-16/2004.
20. “Growth of gold nanodendrites by porphyrin photocatalysis” Wang, Z.; Qiu, Y.; Singh, A.; Shelnutt, J. A., 3rd International Conference on Porphyrins and Phthalocyanines, New Orleans, LA, 7/11-16/2004.

Statement of Unspent Funds Expected at the End of the Period:

Estimated unexpended funds at the end of the budget period are anticipated to be $0K.

Description of Special Recognitions Received by the PIs:

Member of Editorial Board of *Nanotechnology*, IOP, London.

4.4 Subcontract or Consortium Arrangements

Subcontract to the University of New Mexico for instrument time on electron microscopes located in the Departments of Earth & Planetary Sciences and Chemical & Nuclear Engineering.

Chemicals, supplies	$3K
SEM	$5K
TEM	$15K
Total	$23K

5.0 Literature

Cited literature

1. Ahmadi, T. S.; Wang, Z. L.; Green, T. C.; Henglein, A.; El-Sayed, M. A. *Science* **1996,** 272, 1924-1926.
2. Krüger, W.; Fuhrhop, J.-H. *Angew. Chem. Int. Ed. Engl.* **1982,** 21, 131-131.
3. Shelnutt, J. A. *J. Am. Chem. Soc.* **1983,** 105, 7179-7180.
4. Song, Y.; Yang, Y.; Medforth, C. J.; Pereira, E.; Singh, A. K.; Xu, H.; Jiang, Y.; Brinker, C. J.; van Swol, F.; Shelnutt, J. A. *J. Am. Chem. Soc.* **2004,** 126, 635-645.
5. Scharbert, B.; Zeisberger, E.; Paulus, E. *J. Organomet. Chem.* **1995,** 493, 143-147.
6. Itoe, R. N.; Wesson, G. D.; Kalu, E. E. *J. Electrochem. Soc.* **2000,** 147, 2445-50.
7. Mello, R. M. Q.; Ticianelli, E. A. *Electrochim. Acta* **1997,** 42, 1031-1039.
8. Perez, J.; Gonzalez, E. R.; Ticianelli, E. A. *Electrochim. Acta* **1998,** 44, 1329-1339.
9. Staehelin, L. A.; Golecki, J. R.; Fuller, R. C.; Drews, G. *Biophys. J.* **1978,** 85, 3173-3186.
10. van Rossum, V.-J.; Steensgaard, D. B.; Mulder, F. M.; Boender, G. J.; Schaffner, K.; Holzwarth, A. R.; de Groot, H. J. M. *Biochemistry* **2001,** 40, 1587-1595.
11. Blankenship, R. E.; Olson, J. M.; Miller, M., *Antenna complexes from green photosynthetic bacteria*. Kluwer Academic Publishers: Dordrecht, The Netherlands, 1995; p 339-435.
12. Olson, J. M. *Photochem. Photobiol.* **1998,** 67, 61-75.
13. Wang, Z.; Medforth, C. J.; Shelnutt, J. A. *J. Am. Chem. Soc.* **2004,** 126, 16720-16721.
14. Wang, Z.; Medforth, C. J.; Shelnutt, J. A. *J. Am. Chem. Soc.* **2004,** 126, 15954-15955.
15. Faul, C. F. J.; Antonietti, M. *Adv. Mater.* **2003,** 15, 673-683.
16. Lauceri, R.; Gurrieri, S.; Bellacchio, E.; Contino, A.; Monsu'scolaro, L.; Romeo, A.; Toscano, A.; Purrello, R. *Supramol. Chem.* **2000,** 12, 193-202.
17. Micali, N.; Romeo, A.; Lauceri, R.; Purrello, R.; Mallamace, F.; Scolaro, L. M. *J. Phys. Chem. B* **2000,** 104, 9416-9420.
18. Shelnutt, J. A. Method for improving product yields in an anionic metalloporphyrin-based artificial photosynthesis system. 4568435, 1986.
19. Song, X.; Miura, M.; Xu, X.; Taylor, K. K.; Majumder, S. A.; Hobbs, J. D.; Cesarano, J.; Shelnutt, J. A. *Langmuir* **1996,** 12, 2019-2027.
20. Koti, A. S. R.; Taneja, J.; Periasamy, N. *Chem. Phys. Lett.* **2003,** 375, 171-176.
21. Debe, M. K., Novel catalysts, catalysts support and catalysts coated membrane methods. In *Handbook of Fuel Cells -- Fundamentals, Technology and Applications*, Vielstich, W.; Gasteiger, H. A.; Lamm, A., Eds. John Wiley & Sons, Ltd.: New York, 2003; Vol. 3, pp 576-589.
22. Holten, D.; Bocian, D. F.; Lindsey, J. S. *Acc. Chem. Res.* **2002,** 35, 57-69.
23. Kim, D.; Osuka, A. *Acc. Chem. Res.* **2004,** 37, 735-745.
24. Lammi, R. K.; Ambroise, A.; Balasubramanian, T.; Wagner, R. W.; Bocian, D. F.; Holten, D.; Lindsey, J. S. *J. Am. Chem. Soc.* **2000,** 122, 7579-7591.
25. Taniguchi, M.; Ra, D.; Kirmaier, C.; Hindin, E.; Schwartz, J. K.; Diers, J. R.; Knox, R. S.; Bocian, D. F.; Holten, D. *J. Am. Chem. Soc.* **2003,** 125, 13461-13470.
26. Roberts, J. A.; Holten, D.; Kirmaier, C. *J. Phys. Chem. B* **2001,** 105, 5575-5584.
27. Chen, L.; Holten, D.; Bocian, D. F.; Kirmaier, C. *J. Phys. Chem.* **2004,** 108, 10457-10464.
28. Ambroise, A.; Kirmaier, C.; Loewe, R. S.; Bocian, D. F.; Holten, D.; Lindsey, J. S. *J. Org. Chem.* **2002,** 67, 3811-3826.
29. Nakamura, Y.; Hwang, I.-W.; Aratani, N.; Ahn, T. K.; Ko, D. M.; Takagi, A.; Kawai, T.; Matsumoto, T.; Kim, D.; Osuka, A. *J. Am. Chem. Soc.* **2004,** ASAP aticles on web.
30. Sazanovich, I. V.; Kirmaier, C.; Hindin, E.; Yu, L. H.; Bocian, D. F.; Lindsey, J. S.; Holten, D. *J. Am. Chem. Soc.* **2004,** 126, 2664-2665.
31. Bruggemann, B.; Herek, J. L.; Sundstrom, V.; Pullerits, T.; May, V. *J. Phys. Chem. B* **2001,** 105, 11391-11394.
32. Bradforth, S. E.; Jimenez, R.; van Mourik, F.; van Grondelle, R.; Fleming, G. R. *J. Phys. Chem.* **1995,** 99, 16179-16191.
33. Song, X. Z.; Jaquinod, L.; Jentzen, W.; Nurco, D. J.; Jia, S. L.; Khoury, R. G.; Ma, J. G.; Medforth, C. J.; Smith, K. M.; Shelnutt, J. A. *Inorg. Chem.* **1998,** 37, 2009-2019.
34. Song, X. Z.; Jentzen, W.; Jaquinod, L.; Khoury, R. G.; Medforth, C. J.; Jia, S. L.; Ma, J. G.; Smith, K. M.; Shelnutt, J. A. *Inorg. Chem.* **1998,** 37, 2117-2128.
35. Song, X. Z.; Jentzen, W.; Jia, S. L.; Jaquinod, L.; Nurco, D. J.; Medforth, C. J.; Smith, K. M.; Shelnutt, J. A. *J. Am. Chem. Soc.* **1996,** 118, 12975-12988.

36. Sparks, L. D.; Anderson, K. K.; Medforth, C. J.; Smith, K. M.; Shelnutt, J. A. *Inorg. Chem.* **1994,** 33, 2297-2302.
37. Sparks, L. D.; Medforth, C. J.; Park, M. S.; Chamberlain, J. R.; Ondrias, M. R.; Senge, M. O.; Smith, K. M.; Shelnutt, J. A. *J. Am. Chem. Soc.* **1993,** 115, 581-592.
38. Jentzen, W.; Simpson, M. C.; Hobbs, J. D.; Song, X.; Ema, T.; Nelson, N. Y.; Medforth, C. J.; Smith, K. M.; Veyrat, M.; Mazzanti, M.; Ramasseul, R.; Marchon, J. C.; Takeuchi, T.; Goddard, W. A.; Shelnutt, J. A. *J. Am. Chem. Soc.* **1995,** 117, 11085-11097.
39. Shelnutt, J. A., Molecular simulations and normal-coordinate structural analysis of porphyrins and heme proteins. In *The Porphyrin Handbook*, Kadish, K. M.; Smith, K. M.; Guilard, R., Eds. Academic Press: New York, 2000; Vol. 7, pp 167-223.
40. Shelnutt, J. A. *J. Porphyrins Phthalocyanines* **2000,** 4, 386-389.
41. Shelnutt, J. A.; Medforth, C. J.; Berber, M. D.; Barkigia, K. M.; Smith, K. M. *J. Am. Chem. Soc.* **1991,** 113, 4077-4087.
42. Shelnutt, J. A.; Rousseau, D. L.; Dethmers, J. K.; Margoliash, E. *Biochemistry* **1981,** 20, 6485-97.
43. Shelnutt, J. A.; Song, X. Z.; Ma, J. G.; Jia, S. L.; Jentzen, W.; Medforth, C. J. *Chem. Soc. Rev.* **1998,** 27, 31-41.
44. Hobbs, J. D.; Majumder, S. A.; Luo, L.; Sickelsmith, G. A.; Quirke, J. M. E.; Medforth, C. J.; Smith, K. M.; Shelnutt, J. A. *J. Am. Chem. Soc.* **1994,** 116, 3261-3270.
45. Hobbs, J. D.; Shelnutt, J. A. *J. Prot. Chem.* **1995,** 14, 19-25.
46. Haddad, R.; Gazeau, S.; Pécaut, J.; Marchon, J. C.; Medforth, C. J.; Shelnutt, J. A. *J. Am. Chem. Soc.* **2003,** 125, 1253-1268.
47. Song, Y.; Haddad, R.; Jia, S. L.; Hok, S.; Olmstead, M. M.; Nurco, D. J.; Schore, N. E.; Zhang, J.; Ma, J.-G.; Smith, K. M.; Gazeau, S.; Pecaut, J.; Marchon, J. C.; Medforth, C. J.; Shelnutt, J. A. *J. Am. Chem. Soc.* **2005,** 127, 1179-1192.
48. Song, Y.; Challa, S. R.; Medforth, C. J.; Qiu, Y.; Watt, R. K.; Peña, D.; Miller, J. E.; van Swol, F.; Shelnutt, J. A. *Chem. Commun.* **2004**, 1044-1045.
49. van Swol, F.; Woodcock, L. V. to be published.